Austrian Journal of Earth Sciences | Volume 104/2 | 22 - 46 | Vienna | 2011

Emplacement of an evaporitic mélange nappe in central Northern Calcareous Alps: evidence from the Moosegg klippe (Austria)

Anja SCHORN*) & Franz NEUBAUER

KEYWORDS

thin-skinned tectonics
deformation analysis
sulphate mélange
fold-thrust belt
mylonite

Dept. Geography and Geology, University of Salzburg, Hellbrunnerstr. 34, A-5020 Salzburg, Austria;
*) Corresponding author, anja.schorn2@stud.sbg.ac.at

Abstract

For the reconstruction of Alpine tectonics, the Permian to Lower Triassic Haselgebirge Formation of the Northern Calcareous Alps (NCA) (Austria) plays a key role in: (1) understanding the origin of Haselgebirge bearing nappes, (2) revealing tectonic processes not preserved in other units, and (3) in deciphering the mode of emplacement, namely gravity-driven or tectonic. With these aims in mind, we studied the sulphatic Haselgebirge exposed to the east of Golling, particularly the gypsum quarry Moosegg and its surroundings located in the central NCA. There, overlying the Lower Cretaceous Rossfeld Formation, the Haselgebirge Formation forms a tectonic klippe (Grubach klippe) preserved in a synform, which is cut along its northern edge by the ENE-trending high-angle normal Grubach fault juxtaposing Haselgebirge to the Upper Jurassic Oberalm Formation. According to our new data, the Haselgebirge bearing nappe was transported over the Lower Cretaceous Rossfeld Formation, which includes many clasts derived from the Haselgebirge Fm. and its exotic blocks deposited in front of the incoming nappe. The main Haselgebirge body contains foliated, massive and brecciated anhydrite and gypsum. A high variety of sulphatic fabrics is preserved within the Moosegg quarry and dominant gypsum/anhydrite bodies are tectonically mixed with subordinate decimetre- to meter-sized tectonic lenses of dark dolomite, dark-grey, green and red shales, pelagic limestones and marls, and abundant plutonic and volcanic rocks as well as rare metamorphic rocks. At the base of the Haselgebirge Fm., strongly foliated fine-grained anhydrite-carbonate mylonite is preserved together with a WNW-trending stretching lineation together constituting an L-S fabric. This indicates emplacement of the Haselgebirge evaporite mélange under ductile conditions of anhydrite and fine-grained calcite. In other places at the base of the Haselgebirge, anhydrite is transformed into foliated gypsum leaving behind a still well preserved L-S fabric. Foliated and stretched gypsum clasts are quite common, and some of these breccia lenses and their clasts have again been foliated and stretched, implying several stages of ductile deformation. Because of peculiar fabrics, we interpret the formation of gypsum and anhydrite breccia as a result of fluid overpressure, possibly in part related to dehydration reactions of gypsum to anhydrite.

The structural development of the Grubach klippe and of its underlying units reflects a succession of deformation stages ranging from Early Cretaceous to Pliocene. They monitor the structural history from initial late Early Cretaceous nappe stacking within the NCA through emplacement of the NCA onto footwall units during Eocene collision of the Austroalpine nappe stack with the European foreland, an early hitherto undetected stage of orogenic collapse with NW-SE transtension, as well as various stages of lateral extrusion of central sectors of Eastern Alps. Consequently, local data in a high level of an orogen can be taken to monitor major kinematic stages of an entire orogen.

Für die Rekonstruktion der alpinen Tektonik spielt die permische bis untertriassische Haselgebirge-Formation der Nördlichen Kalkalpen (Österreich) eine Schlüsselrolle. Sie führt potentiell primäre oder tektonische Einschlüsse von magmatischen und metamorphen Gesteinen, die in keinen anderen ostalpinen Einheiten erhalten sind. Diese zeigen daher Hinweise auf die Herkunft der Haselgebirge-führenden tektonischen Decken und auf die tektonischen Prozesse der Platznahme, gravitativ oder tektonisch. Die sulphatische Haselgebirge-Mélange östlich von Golling, insbesondere der Moosegg Gips-Steinbruch und seine nähere Umgebung in den zentralen Nördlichen Kalkalpen wurden mit besonderem Augenmerk auf diese Problemstellungen untersucht. Dort bildet die Haselgebirge-Formation, welche die unterkretazische Rossfeld-Formation überlagert, eine tektonische Klippe (Grubach Klippe) in einer Mulde. An ihrem nördlichen Rand wird sie von der ENE-streichenden, steilen Grubach-Abschiebung abgeschnitten, welche die Haselgebirge- Formation und die oberjurassische Oberalm-Formation nebeneinandersetzt. Nach unseren neuen Daten wurde die Haselgebirge-führende Decke über die Rossfeld-Formation geschoben. Dabei wurden viele unterschiedliche Klasten und exotische Blöcke aus den Haselgebirgs-Gesteinen der tiefjuvavischen Decke erodiert und anschließend an der Überschiebungsfront (im Rossfeld-Flexurbecken) abgelagert. Der größte Teil des Haselgebirge-Körpers enthält geschieferten, massigen und brekziierten Anhydrit und Gips.

Im Moosegg-Steinbruch sind verschiedene Typen von sulphatischen Gefügen erhalten. In die dominierenden Gips- und Anhydritkörper sind untergeordnet tektonische dm- bis m-große Linsen von dunklem Dolomit, dunkelgrauen, roten und grünen Tonsteinen, pelagischen Kalken, Mergeln und verschiedensten plutonischen und vulkanischen Gesteinen sowie seltenen Metamorphiten eingelagert. An der Basis der Haselgebirge-Formation sind stark geschieferte, feinkörnige Anhydrit-Karbonat-Mylonite mit einer WNW-

streichenden Streckungslineation und einem L-S-Gefüge aufgeschlossen, welches auf eine Platznahme der Haselgebirge-Evaporit-Mélange unter duktilen Bedingungen von Anhydrit und feinkörnigem Calcit) hinweist. Auch in anderen Bereichen an der Basis der Haselgebirge-Formation hinterließ die Umwandlung von Anhydrit in geschieferten Gips durch gut erhaltene L-S-Gefüge. Geschieferte und gestreckte Gipsklasten sind recht häufig und einige der Brekzienlinsen und ihre Klasten wurden ein zweites Mal verschiefert und gestreckt, was auf mehrere Stufen duktiler Deformation hinweist. Aufgrund dieser Gefüge interpretieren wir die Bildung der Gips-und Anhydrit-Brekzie als ein Resultat von Fluidüberdruck, möglicherweise im Zusammenhang mit einer Dehydratisierungsreaktion von Gips zu Anhydrit.

Die strukturelle Entwicklung der Grubach Klippe und ihrer unterlagernden Einheiten spiegelt eine Abfolge von Deformationsereignissen von der Oberkreide bis zum Pliozän wieder. Sie zeigt damit die strukturelle Geschichte von der initialen oberkretazischen Deckenstapelung in den Nördlichen Kalkalpen über deren Platznahme auf den liegenden Einheiten während der eozänen Kollision der ostalpinen Deckenstapeln mit dem europäischen Vorland an. Außerdem lassen sich sowohl ein frühes, bisher unentdecktes Stadium eines orogenen Kollapses mit NW-SE-Transtension als auch verschiedene Stadien lateraler Extrusion in zentralen Bereichen der Ostalpen nachweisen. Somit können lokale strukturelle Daten aus einem hohen Level eines Gebirges verwendet werden, um wesentliche Stadien der kinematischen Entwicklung des gesamten Gebirges nachzuvollziehen.

1. Introduction

Evaporite mélanges often form detachment respectively decollément surfaces of major extensional and contractional allochthons because of their very low shear resistance. Due to the deposition of evaporites during an early stage of passive continental margin formation, they are commonly overlain by thick successions of carbonates and/or siliciclastic rocks from the main thermal subsidence stage of a passive margin, and these rocks are resistant against penetrative internal deformation at moderate temperature conditions (<250 – 300°C). The most common cases of evaporite mélanges are such (1) at passive continental margins, where they are deformed during gravity-driven extension, commonly raft tectonics, in an extensional geodynamic setting (Rouby et al., 2002; Butler and Paton, 2011), and (2) in external foreland fold-thrust belts within a convergent geodynamic setting (Hudec and Jackson, 2006). In the following, we present new structural data from a key area of the central Northern Calcareous Alps (NCA) (Mandl, 2000). Our new data allows a new tectonic interpretation of the central NCA. There, the Haselgebirge is preserved in a tectonic nappe. Ductile Early to possibly early Late Cretaceous fabrics were formed in a tectonic mélange exposed at the structural base of the Haselgebirge nappe. The structural evolution is in line with the surrounding units, and includes thrusting overprinted by extensional and strike-slip tectonic events.

2. Geological setting

The classic division within the NCA defines the Bajuvaric, Tirolic and Juvavic nappe complexes (Tollmann, 1985 and references therein) (Fig. 1). The Permian to Lower Triassic Haselgebirge occurs mainly in Juvavic units of the central and eastern NCA (Schauberger, 1986; Leitner et al., 2011 and references therein). The age of formations in the NCA ranges from Late Carboniferous (?) or Early Permian to Eocene. During the Middle and Late Triassic, the Upper Juvavic nappes comprise mostly reefs and deposits next to reefs.

The Tirolic and Bajuvaric nappes comprise lagoonal facies types and subordinate reefs. The Lower Juvavic nappe unit represents solely an outer shelf or a deep-sea facies type (Mandl, 2000). Rocksalt deposits are mostly found in the Lower Juvavic unit. Sedimentation of the Lower Juvavic unit occurred in basins with basinal limestones (Pötschen Limestone) and on intrabasinal ridges, with reduced sedimentary thickness (the pelagic Hallstatt Limestone). The ridges were suggested to relate to salt diapirism in Triassic times (Plöchinger, 1984; Mandl, 1982, 2000).

The westernmost part of the expanding Triassic Tethys ocean is called Hallstatt-Meliata Ocean, which comprises rare deep sea (ophiolitic?) sequences in the eastern parts of the NCA (Faupl and Wagreich, 2000; Neubauer et al., 2000 and references therein). Most authors interpret the Hallstatt Limestone as an outer shelf (Tollmann, 1987; Mandl, 2000). Others propose a position of the Hallstatt-Meliata relics between the Upper Juvavic and Tirolic units (Schweigl and Neubauer, 1997). The Hallstatt-Meliata Ocean was being closed during the Late Jurassic (Dallmeyer et al., 2008 and references therein). Coevally, the sea floor dropped and reached maximum water depths with the formation of radiolarites. Gravitational sliding is reported from different places (e.g., Plöchinger, 1990; Mandl, 1982), and this concept was developed until recent years (Missoni and Gawlick, 2011 and references therein). These authors argue for a Late Jurassic age of shortening.

During Early Cretaceous, nappe stacking of Austroalpine units started due to the subduction of Austroalpine continental crust. Thrusting prograded from south to north, respectively from ESE to WNW (Ratschbacher, 1986; Linzer et al., 1995; Neubauer et al., 2000; Mandl, 2000).

The mechanism and the time of emplacement of the Juvavic units are still a matter of controversy. The classic hypothesis assumes that both Juvavic nappes took their position during the eo-Alpine deformational event (late Early to early Late Cretaceous) by means of thrust tectonics (Kober, 1955; Pichler, 1963; Schweigl and Neubauer, 1997). A further model explains the emplacement of all Juvavic units by gravity sliding since Late Jurassic times, as Haselgebirge clasts of various size have been found in the Upper Jurassic Oberalm and Lower Cretaceous Rossfeld formations (Missoni and Gawlick, 2011 and references therein). This concept was extended to large mountain-like blocks also explained by emplacement by simple

gravity sliding (Gawlick and Lein, 2000; Missoni and Gawlick, 2011 and references therein). Frank and Schlager (2006) propose the emplacement as a consequence of Late Jurassic strike-slip movements related to the opening of the Penninic Ocean.

In the Eocene, the second paroxysm of Alpine orogeny occurred, when continental basement slices ("Middle Penninic") and parts of the North Penninic Ocean ("Rhenodanubian Flysch") were subducted below the NCA at the leading edge of the Austroalpine-Adriatic microcontinent (Faupl and Wagreich, 2000;

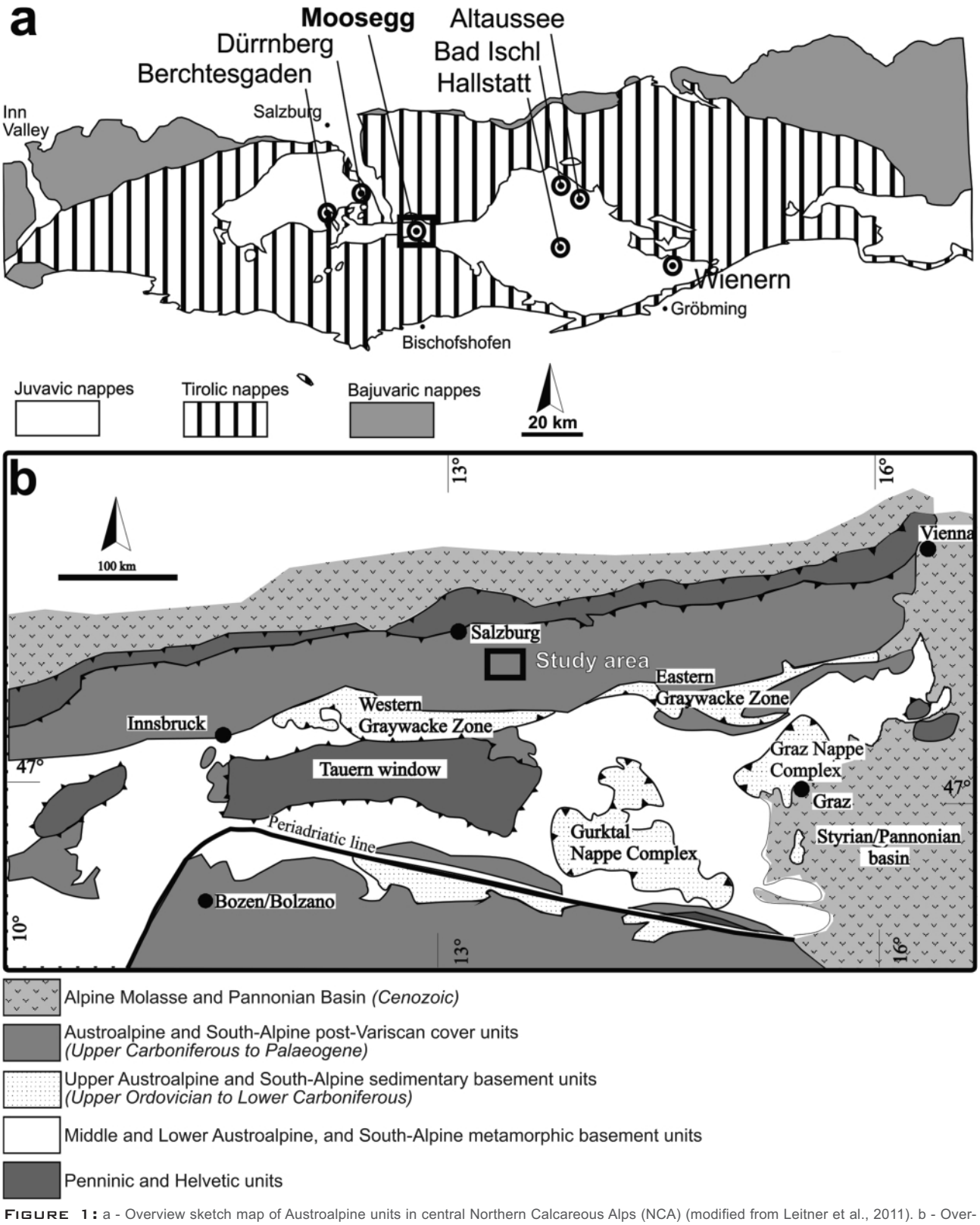

Figure 1: a - Overview sketch map of Austroalpine units in central Northern Calcareous Alps (NCA) (modified from Leitner et al., 2011). b - Overview of Austroalpine units in Eastern Alps.

In the Eocene, the second paroxysm of Alpine orogeny occurred, when continental basement slices (“Middle Penninic”) and parts of the North Penninic Ocean (“Rhenodanubian Flysch”) were subducted below the NCA at the leading edge of the Austroalpine-Adriatic microcontinent (Faupl and Wagreich, 2000; Linzer et al., 2002 and references therein). The present NCA were partly detached from their Austroalpine basement (e.g., Greywacke zone) and thrusted over the Rhenodanubian Flysch

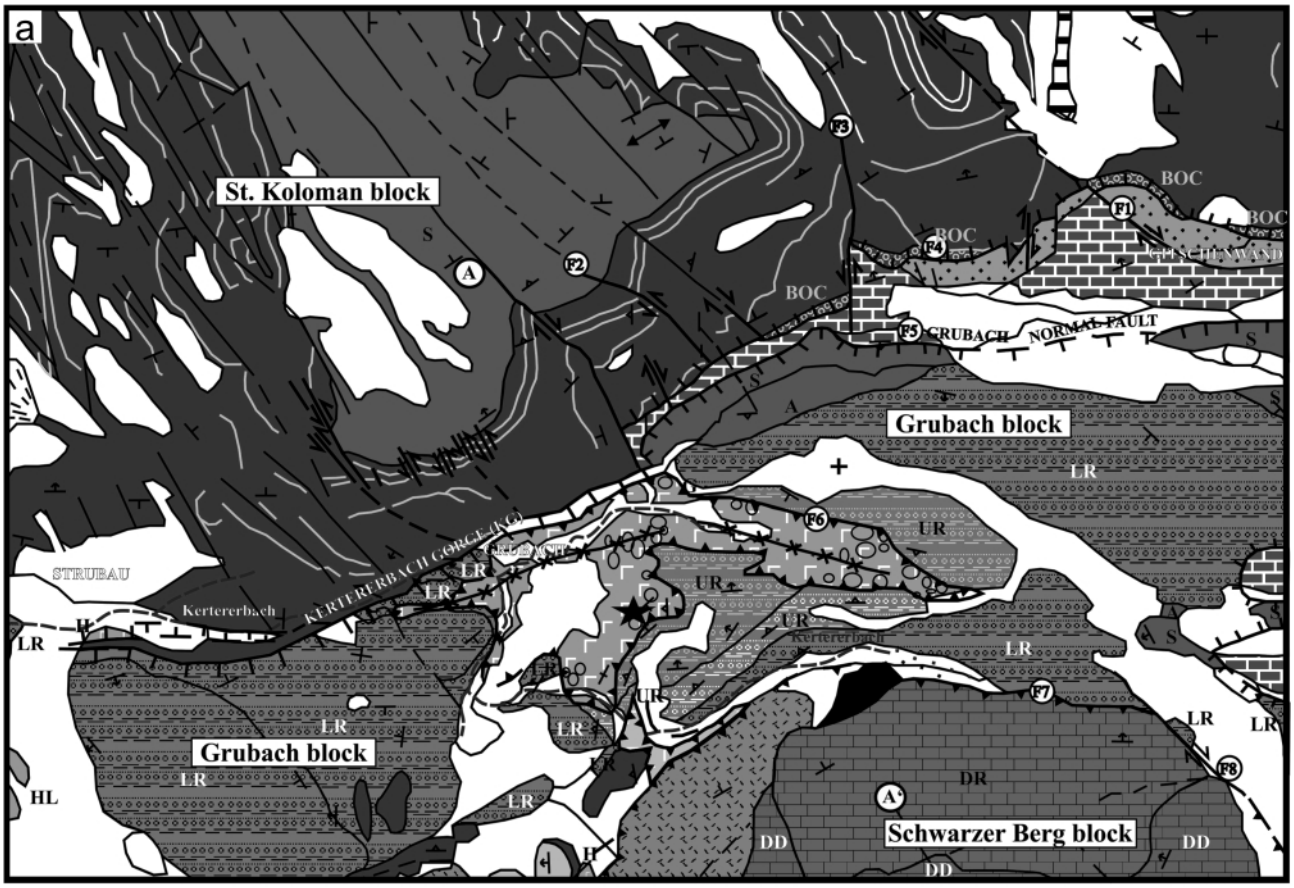

Figure 2a: Geological map of the central southern part of the Osterhorn Tirolic nappe and overlying units (modified after Geological Map, scale 1:50,000, sheet Hallein (Plöchinger, 1987) updated by own observations. F1 – F8 denotes major faults (see text for explanation). KG, location of Kertererbach gorge. A - A´, section of Figure 2b.

and Helvetic domain resulting in a wide thin-skinned tectonic nappe complex (Linzer et al., 1995; Mandl, 2000; Neubauer et al., 2000). The familiar rocksalt deposits, which are all located in the interior of the NCA mostly within the Lower Juvavic unit, were considered to be only slightly affected by these Cenozoic deformation stages, since the detachment of the NCA domain occurred beneath the lowermost unit, the Bajuvaric nappe (Fig. 1). Deformation of Upper Cretaceous to Eocene Gosau basins deposited on uppermost nappes (Tirolic and Juvavic nappes) suggests significant deformation in Late Eocene to Early Miocene (Linzer et al., 1995, 1997; Peresson and Decker, 1997a, b). Numerous data regarding these brittle deformation stages of the central and eastern NCA has been presented by Decker et al. (1992), Linzer et al. (1997), Peresson and Decker (1997a, b) and Schweigl and Neubauer (1997). We here use the succession of deformational stages established by Peresson and Decker (1997a, b) because the timing of their succession is constrained by sediments exposed in the eastern NCA.

3. Regional geology of central Northern Calcareous Alps

The study area is located in the central NCA (Fig. 1). There, the Bajuvaric units only form a small rim along northern margins of the NCA. The flat-lying Tirolic units are widespread within the so-called Tirolic Arc (Tirolischer Bogen). The Juvavic units are divided into the Lower Juvavic unit with the Haselgebirge Fm. and mainly lenses and blocks of Middle-Upper Triassic pelagic limestone of the Hallstatt facies realm (Tollmann, 1987). These units are tectonically overlain by the Upper Juvavic units of the Untersberg and Dachstein nappes, which mainly comprise thick Middle Triassic shallow-water Wetterstein Dolomite/Limestone and its Upper Triassic lagoonal and reef limestones of the Dachstein Formation.

4. Lithology of the Moosegg klippe

An overview on the study area and a section is shown in Figure 2a. The gypsum mine Grubach at Moosegg (Figs. 3, 4a) was first documented in 1613. In the course of our research, the Moosegg quarry was mapped in detail in terms of its geology (Figs. 3, 4a). The levels of the quarry were numbered from I to X with increasing altitude.

In principle, the main parts of the quarry are composed of a partly karstified cap of gypsum (Fig. 4a and b). A synform of light-coloured massive gypsum with lenses of anhydrite in the centre is surrounded by more or less foliated dark gypsum breccia. Furthermore, some decimetre- to meter-sized blocks of exotic rocks including different types of plutonic rocks, greenstones and various claystones/mudstones as well as dolomite

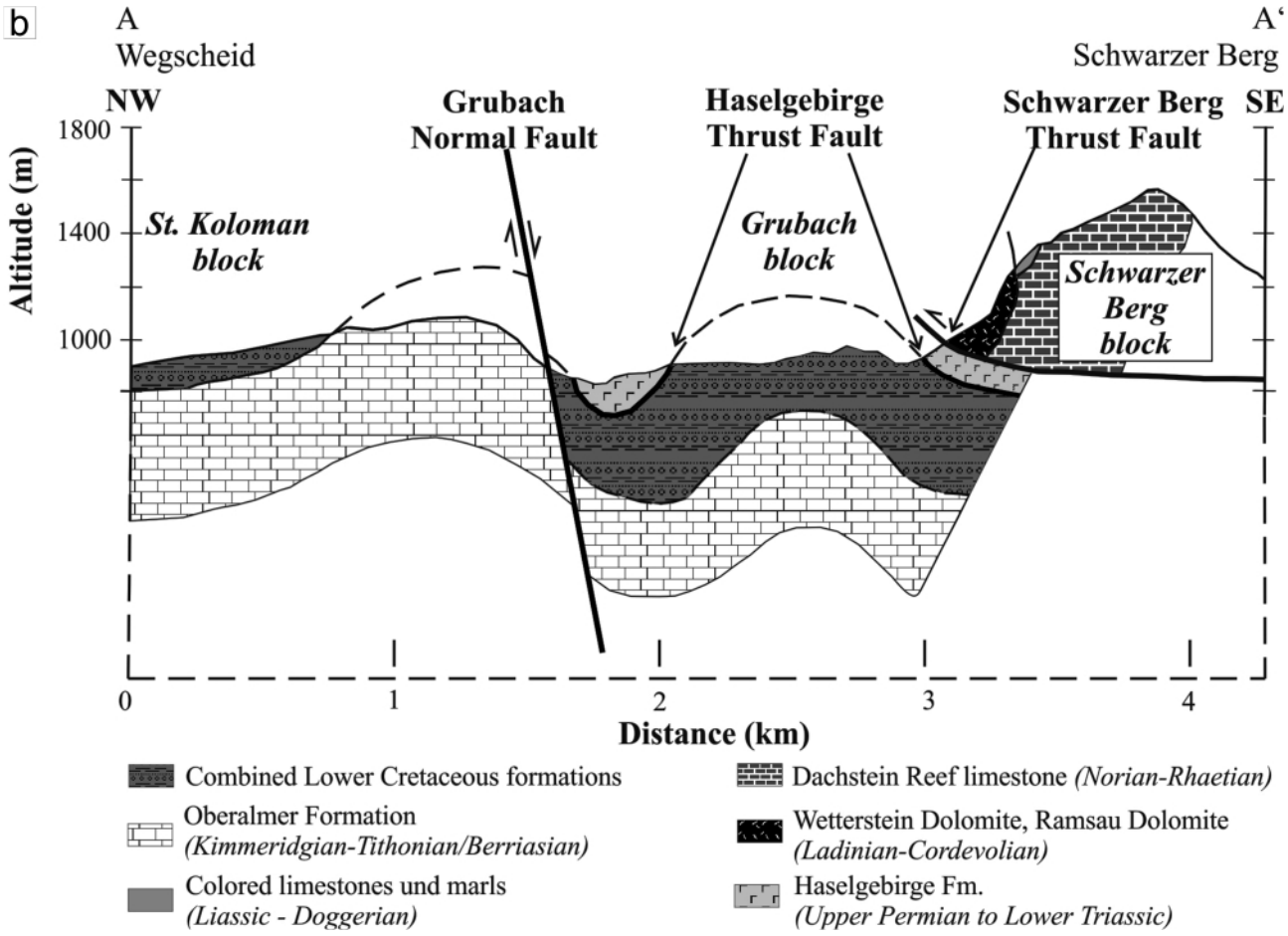

Figure 2b: Simplified NW-trending section across the study area showing the Moosegg klippe, the Grubach normal fault, the Haselgebirge thrust fault, synclines anticlines and the Schwarzer Berg thrust fault.

lenses are of great importance. In the following, the principal rock types are briefly described.

Light-coloured massive gypsum and anhydrite: As mentioned above the light gypsum occurs in a synform in the centre of the Moosegg quarry (Fig. 4a). It is commonly massive and only in the upper rim partially foliated. Furthermore, some lenses of darker and internally strongly foliated coarse-grained anhydrite are interbedded (Fig. 4a).

Gypsum breccia: The gypsum breccia (Fig. 4a and c) constitutes the bulk of the quarry. In the lower and eastern sectors, the breccia is lighter in colour and exhibits only a weak foliation. In the upper eastern as well as in the entire western area the rock is darker and in part strongly foliated. Particularly, the upper sectors of the quarry are deeply weathered and exhibit karst phenomena like karst caveats (Fig. 4b). The matrix of the breccia is gypsum. The breccia components vary in size between 1 cm and 1 m. Apart from gypsum and anhydrite they consist of different types of magmatic and metamorphic rocks (Fig. 4d). We found various types of rare ultramafic rocks (serpentinite, pyroxenite), widespread biotite-bearing diorite, metadolerite and meta-syenite, as well as rare metamorphic, banded metapsammitic schists and meta-doleritic blueschists. These rocks, their geochemical compositions and $^{40}Ar/^{39}Ar$ mineral ages are described in a companion paper (Schorn et al., submitted, see also Schorn, 2010).

Dark gypsum breccia with two types of dark components: The strongly foliated gypsum breccia contains two types of dark components (Fig. 4d). Lenses of the first type are composed of cataclastically deformed, broken dark dolomite, which are rich in veins of white gypsum and very sulphurous in the middle/centre of the lenses. The second type consists of banded/laminated siliceous mudstone. Furthermore, some well preserved biotite-diorite blocks (Fig. 4d) also occur in the breccia.

Gypsum mylonite (base of the Haselgebirge nappe): The dark gypsum mylonite (Fig. 8) was completely fractured during thrusting and crops out in the eastern parts of levels VII and VIII.

Upper Rossfeld Formation: The quartz-rich, carbonate-cemented dark sandstones of the Upper Rossfeld Formation represent several decimetre thick layers intercalated with thin mudstones. These sandstones are exposed on the south-western edge of the Moosegg quarry, underlying the gypsum mylonite (Fig. 3). The sandstones are interpreted to represent turbidites (e.g., Faupl and Tollmann, 1978). The tectonic contact with the gypsum breccia is not directly exposed in the forest but many blocks of gypsum mylonite (Fig. 3) are found in a short distance from sandstones of the Upper Rossfeld Formation.

4.1 Blocks within the gypsum breccia

In the following, various blocks from the gypsum breccia are described beside the above mentioned magmatic and metamorphic blocks. All these blocks are fully embedded within a gypsum matrix. These lenticular tectonic blocks occur in all sizes between several centimetres and tens of metres. The foliated dark gypsum breccia (Fig. 4l) represents a zone, which is located on the western part of level V and consists of a groundmass of dark gypsum with small components of light-coloured and red gypsum, anhydrite and different types of magmatic, mostly green-coloured rocks (e.g. serpentinite). The

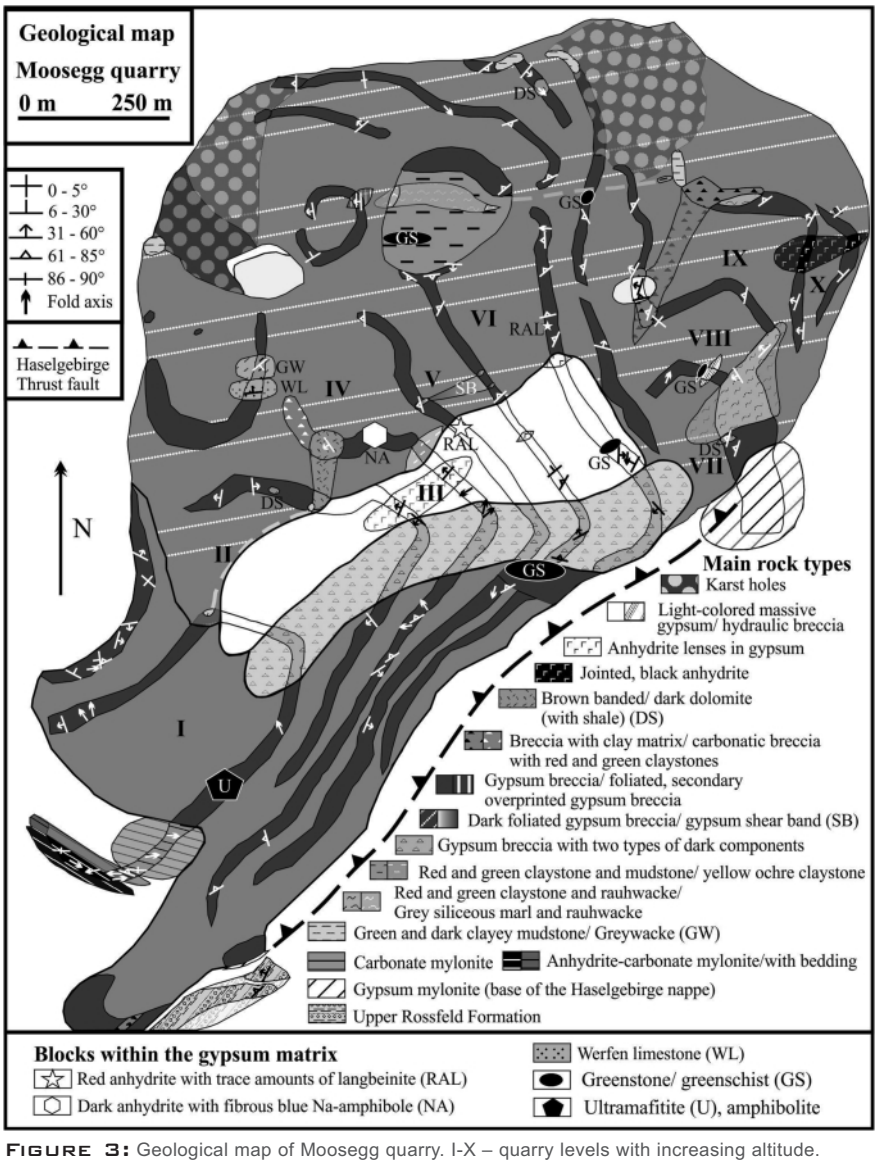

Figure 3: Geological map of Moosegg quarry. I-X – quarry levels with increasing altitude.

components show in part a differently orientated foliation compared with the matrix, indicating a secondary transposition respectively overprint of the earlier formed foliation. These also indicate at least two different stages of deformation. Grey siliceous marl is strongly weathered and only occurs as a lens in the red and green claystone of level VI. Rauhwacke is also strongly weathered and only occurs as a lens in the red and green claystone of level VI (Fig. 4e). Ultramafitite is also only exposed as a small lens within the red and green claystone of level VI. Beside serpentine, few brownish pyroxene grains can be observed. Red and green claystone / mudstone and partly siliceous claystones form the bulk of a non-mined hill in the

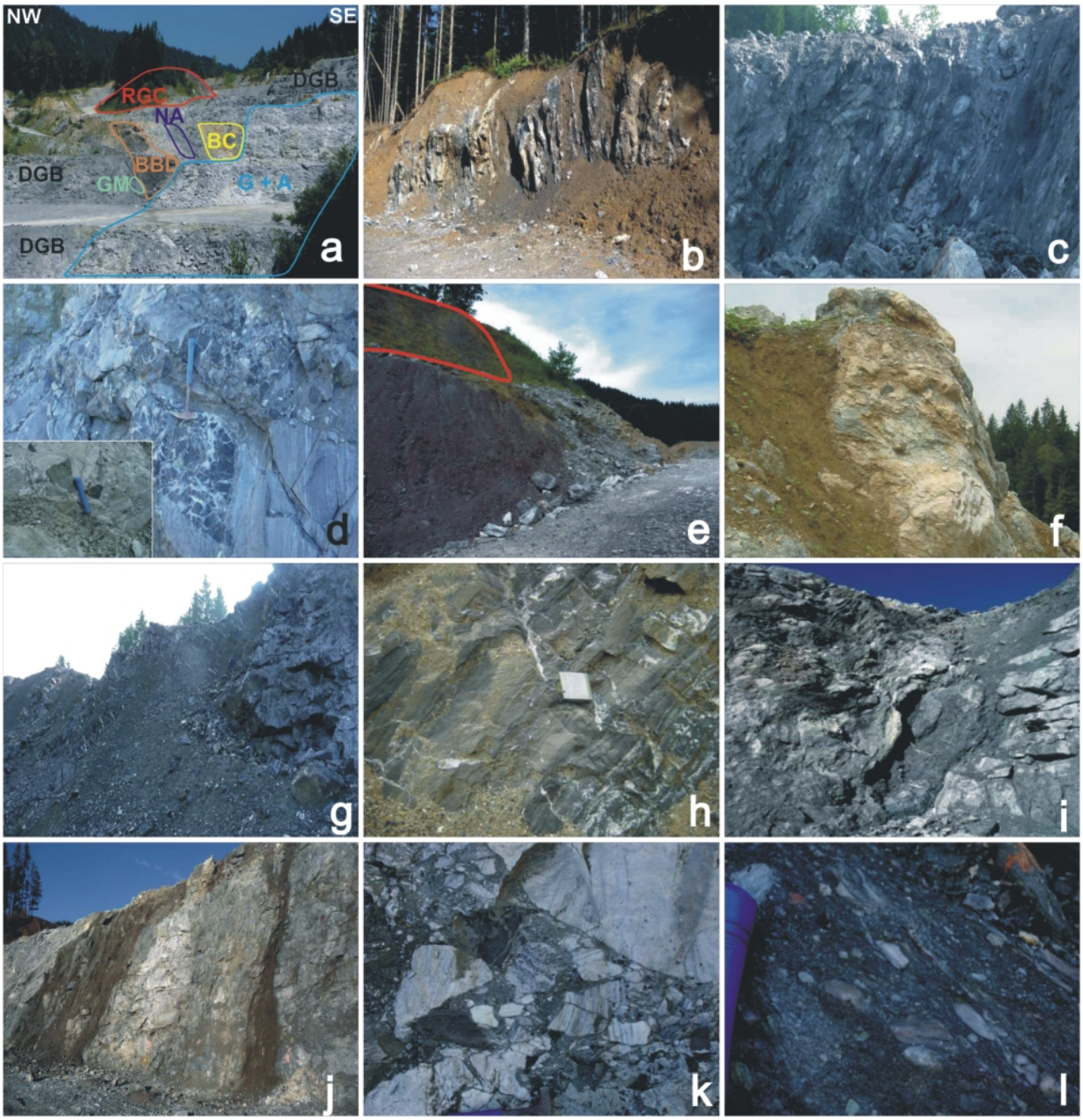

Figure 4: Field photographs from the lithologies in the Moosegg quarry. a - Overview of Moosegg quarry: Note the lenses of brown, banded dolomite (BBD), green and dark clayey mudstone (GM), light-brownish claystone (BC), dark anhydrite with fibrous blue Na-amphibole (NA) and red and green claystone (RGC) on the left side and light-coloured white gypsum (G) with small lenses of anhydrite (A) on the right side, embedded in dark, foliated gypsum breccia (DGB). b - Karst caveats in the uppermost part of the quarry. c - Strongly foliated gypsum breccia of level VIII. d - Dark gypsum breccia with two types of dark components; the small pictures shows a well preserved biotite-diorite block. e - Boundary between grey siliceous marl and rauhwacke (cellular limestone; upper side) and red and green claystone and mudstone. f - Carbonatic breccia with red and green claystone and mudstone. g - Dark jointed anhydrite. h - Brown banded dolomite of level III. i - Dark anhydrite with fibrous blue amphibole. j - Shear zones of level V. k - Hydraulic gypsum breccia of level IV with foliated gypsum clasts and unfoliated matrix. Note also the fit of some clasts in center of the image indicating hydraulic brecciation. l - Foliated dark gypsum breccia of level V, indicating a second stage of foliation postdating brecciation and, therefore, two stages of deformation.

north-western part of level VI (Fig. 4e). The claystones are of variable colour and often laminated. These rocks were often considered as siltstones of the Werfen Formation. However, the lamination and missing detrital white mica in some areas as well as the siliceous contents disprove this correlation. We do not exclude that the northern part of this hill comprises mica-bearing mudstones of the Werfen Formation. The red and green claystones and mudstones may represent abyssal deposits with a possible origin in the Meliata Ocean. Further chlorite-rich greenstones occur on the southern side of the

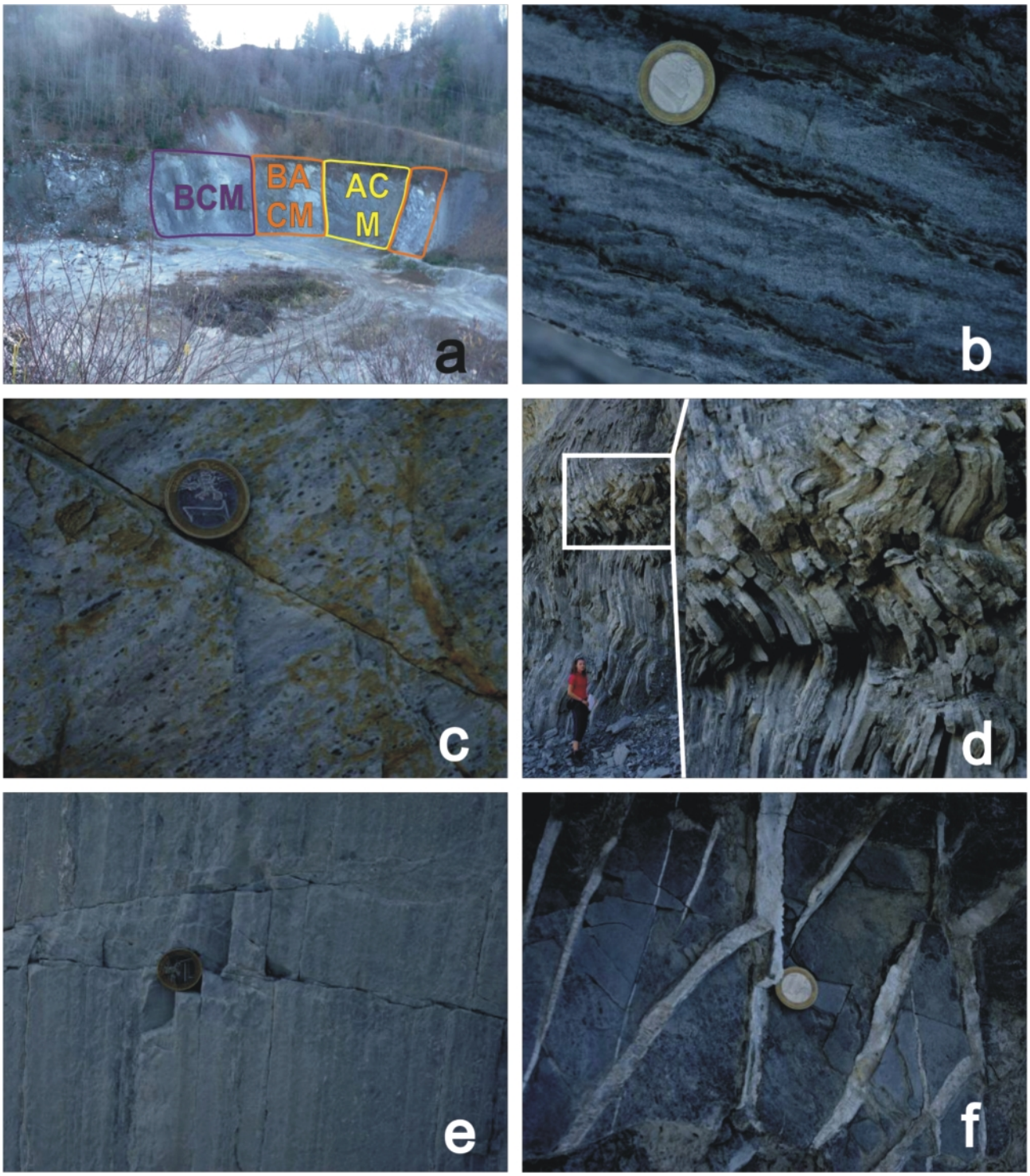

Figure 5: a - Overview of the southern part of level I with BCM - banded carbonate mylonite, BACM - banded anhydrite-carbonate mylonite and ACM – anhydrite-carbonate mylonite. b - Foliation in banded anhydrite-carbonate mylonite. The foliation S1 intersects bedding with an acute angle. c - Stretching lineation in anhydrite-carbonate mylonite. The stretching lineation is underlined by elongated rigid pyrite porphyroclasts with pressure fringes subparallel to the stretching lineation. d - Well foliated banded anhydrite-carbonate mylonite with folds at level I of the Moosegg quarry. e - A peculiar case of the fracture cleavage S2 in well foliated carbonate mylonite. f - Gypsum-filled extensional veins. Note two sets of veins and a similar orientation of fibers in both sets; for explanation, see text.

mentioned hill.

The thin-bedded, brownish micaceous greywacke is intercalated by shale and is located on the western rim of level III and can also be interpreted as an abyssal deposit. Bedded brownish micritric limestones are preliminary assigned to the Werfen Limestone Formation. In the western part of the levels IV and VIII, dark brownish to dark grey, laminated, decimetre-thick layers of dolomite grade into dark shale. Carbonatic breccia (with red and green claystone) only crops out in the western part of level III (Fig. 4f) and is presumably a tectonic breccia. It was likely formed during deformation associated with emplacement of the Haselgebirge nappe (see below). A tectonic breccia with clay matrix is located on the central part of the levels VIII and IX. The dark grey matrix consists of a mixture of clay and gypsum. Most notably on the boundary to light-coloured massive gypsum and the foliated gypsum breccia the rock shows a loamy-clayish ("letten"-like) cover and thin shear bands. The components, mainly white, red, light and dark coloured gypsum and anhydrite, vary in size from centimetre to meter and are partly cleaved.

Dark grey to nearly black jointed anhydrite is very rich in thin white gypsum joints (Fig. 4g). It is mainly exposed in the north-eastern part of level IX, and subordinately and strongly weathered also in level X. The brown, banded dolomite shows a dark brown lamination (Fig. 4h) and is located in the western part of levels II and III. This rock has never been described before as a part of the Haselgebirge nappe and is quite rich in extension joints and blue Na-amphibole (riebeckite according to unpublished microprobe analyses; Bernroider et al., in prep.). Lenses of dark anhydrite with extension veins filled by fibrous blue amphibole are located in the western part of level III (Fig. 4i). The occurrence of the blue amphibole is likely a result of rock/hydrothermal brine interaction.

The light, yellow ochre-coloured, brownish weathered and bedded claystone only crops out in the western part of level III adjacent to the dark anhydrite with fibrous blue amphibole and massy light gypsum.

Green and dark clayey mudstones are strongly weathered rocks and only occur in the western parts of levels II, IV, VIII and IX, partly together with karst caveats. The occurrence of strongly weathered red and green claystone and rauhwacke are restricted to the north-eastern part of the levels VII, VIII and IX. Chlorite-rich greenstones and greenschists are found in levels IV, V and VI, always within partially strongly weathered lenses of the dark gypsum breccia.

Hydraulic breccia (Fig. 4k) with foliated clasts and an unfoliated gypsum matrix mainly occurs in the south-eastern part of levels IV and VII. Because of the relationship of foliated gypsum clasts in an unfoliated gypsum matrix we assume a fluid-assisted brecciation postdating ductile deformation of sulphates. The origin of the water could be explained by conversion of gypsum to anhydrite (temperature between 42 and 125° C; Murray, 1964).

A variety of millimetre-banded mylonites including carbonate mylonite, banded anhydrite-carbonate-mylonite and anhydrite mylonite occurs in the south-eastern part of level I (Fig. 5a-f). They represent a succession of thinly banded and foliated mylonites of variable composition. The carbonate mylonite comprises millimetre-sized pyrite grains with pressure fringes indicating a well-expressed stretching lineation (Fig. 5c). The banded mylonites are nearly vertically or steeply N-dipping, and shear criteria indicate a top west movement of the Haselgebirge nappe. The foliation is folded (Fig. 5d). For details on these peculiar rocks, see chapter 5.2.

The magmatic and metamorphic rock boudins within the evaporite mélange have been studied in detail (Schorn et al., submitted). We found various types of (1) widespread biotite-bearing diorite (Fig. 4d), meta-syenite, (2) meta-dolerite and rare ultramafic rocks (serpentinite, pyroxenite), as well as (3) rare metamorphic banded meta-psammitic schists and meta-doleritic blueschists. The $^{40}Ar/^{39}Ar$ biotite from three meta-diorite and three meta-dolerite samples with variable compo-sition and fabrics range from 248 to 270 Ma (e.g., 251.2 ± 1.1 Ma) indicating a Permian age of cooling after magma crystallization. The chemical composition of biotite-diorite and meta-syenite indicate an alkaline trend. We interpret the plutonic rocks to represent a rift-related magmatic suite. We also studied rare metamorphic rocks, particularly a meta-doleritic blueschist of N-MORB origin. The scattered $^{40}Ar/^{39}Ar$ white mica age of one sample is at 349 ± 15 Ma, similar to white mica of a banded meta-psammitic schist (~ 378 Ma), and both ages prove the Variscan age of pressure-dominated metamorphism. This age is in the range of detrital white mica ages reported from the underlying Rossfeld Fm. (Eynatten et al., 1996) indicating a close source-sink relationship.

5. Structures of Moosegg klippe

5.1 Description of the structural map

We updated and reinterpreted map-scale structures of the existing geological map scale 1:50,000, sheet Hallein (Plöchinger, 1987, 1990). In the following, we first describe the main geological units (Fig. 2a):

1. The northern unit (St. Koloman block) is composed of flatlying Upper Jurassic Oberalm and Lower Cretaceous Schrambach formations. To the south, this unit is confined by the Grubach normal fault, which was not interpreted as such until now.
2. The central sector (Grubach block), is composed of Lower Cretaceous Rossfeld, Hochreith and lowermost Upper Cretaceous Grabenwald Formations, which are folded. In a syncline, these formations are overlain by the Upper Permian to Lower Triassic Haselgebirge Formation, which here forms the Moosegg klippe (Fig. 2b). Furthermore, Hauptdolomite and the associated Kössen Fm. are exposed in the footwall of a NNW-dipping respectively SSE-dipping normal fault (the latter is the Grubach normal fault) as well as in the anticlinal cores beneath the Rossfeld Formation.
3. To the south, both the Rossfeld and Haselgebirge formations are overthrusted by the Schwarzer Berg nappe, a block mainly comprising Upper Triassic dolomites (Fig. 2a, b).

In the following, we describe the main map-scale structures and their relative timing based on the reinterpreted tectonic map and section (Fig. 2a, b). In the northwestern block (St. Koloman block), NW-trending strike-slip faults dominate (Fig. 2a). Both dextral (e.g. F1 in Fig. 2a) and sinistral (e.g. F2 in Fig. 2a) offsets occur. Among these, fault F1 (in Fig. 2a) displays a major dextral offset of ca. 1.5 km and this fault F1 also cuts the Grubach normal fault system. Furthermore, a few N-S trending sinistral strike-slip faults (e.g. F3 in Fig. 2a) also occur. Together, the NW-trending dextral and N-trending sinistral faults can be interpreted as conjugate Mohr fractures implying a ca. NNW–SSE orientation of the maximum principal stress axis (consistent with deformation stage D_4, see below) during faulting. The NW-trending sinistral strike-slip faults (e. g. F2) imply ca. E–W compression and an E–W orientation of the maximum principal stress axis (consistent with deformation stage D_7, see below).

A horst structure exposing Hauptdolomite beneath the ca. ENE-trending Grubach normal fault system occurs along the southern edge of the St. Koloman block (Fig. 2a). The northern fault (e.g. F4 in Fig. 2a) is NNW-dipping and the Lower and Middle Jurassic formations are cut out along the fault. We call the SSE-dipping normal fault Grubach normal fault (e.g. F5 in Fig. 2a) and the fault juxtaposes Upper Triassic Hauptdolomite to Lower Cretaceous formations. Under the assumption of orthogonal extension to the strike of the normal faults, this normal fault system implies ca. NNW-SSE extension or transtension (deformation stage D_4, see below).

The central block (Grubach block) exposes the Haselgebirge nappe in two ca. ESE to E-trending synforms, which are separated by antiform structures (Fig. 2a and b). The Haselgebirge nappe forms a klippe. In the easternmost sectors, the Hauptdolomite is exposed beneath the Lower Cretaceous Rossfeld Formation in two antiformal structures. The fault (F6) between these two units can be interpreted either as a normal or a thrust fault but predates folding in both alternative interpretations.

The Schwarzer Berg block in the south overrides both the Haselgebirge and the underlying Rossfeld Formation along a further thrust fault (F7 in Fig. 2a). We tentatively assume that this thrust fault postdates the Haselgebirge thrust. At the northeastern edge, a NW-trending dextral strike-slip fault (F8 in Fig. 2a) cuts the thrust F7, and is therefore younger than the Schwarzer Berg thrust (deformation stage D_{3b} in the sequence explained below).

5.2 Description of structures at level I of Moosegg quarry

In the south-eastern part of level I (Fig. 5a) ductile structures related to thrusting of the Haselgebirge Fm. over Lower to lowermost Upper Cretaceous rocks are preserved in folded, nearly vertically dipping anhydrite and carbonate mylonites (Fig. 5b, d). The anhydrite-carbonate mylonite is 5 – 6 m thick and contains, in the lower part of the outcrop, a lot of pyrite, which shows a distinct stretching lineation (Fig. 5c). Furthermore, the banded mylonite rock comprises ca. 1 – 3 cm wide extension veins filled with in part fibrous gypsum (Fig. 5f). These are arranged in two orientations. The main orientation is subvertical and fibres are oriented sub-perpendicular to vein walls. The subordinate veins are steeply E-dipping, and fibres have a similar orientation as in the main set. The similar orientation of fibres in both sets proves a co-genetic origin of both sets of gypsum-filled extensional veins.

The banded anhydrite-carbonate mylonite (Fig. 5b and d) is exposed with a thickness of about four meters. It consists of ca. 75% of 0.5 – 4 cm thick anhydrite layers, which are separated by 3 - 4 cm thick layers of dark foliated mudstone (Fig. 5b). In addition to the pyrite lineation, we found evidence for an intersecting δ-lineation and evidence for an axial plane foliation.

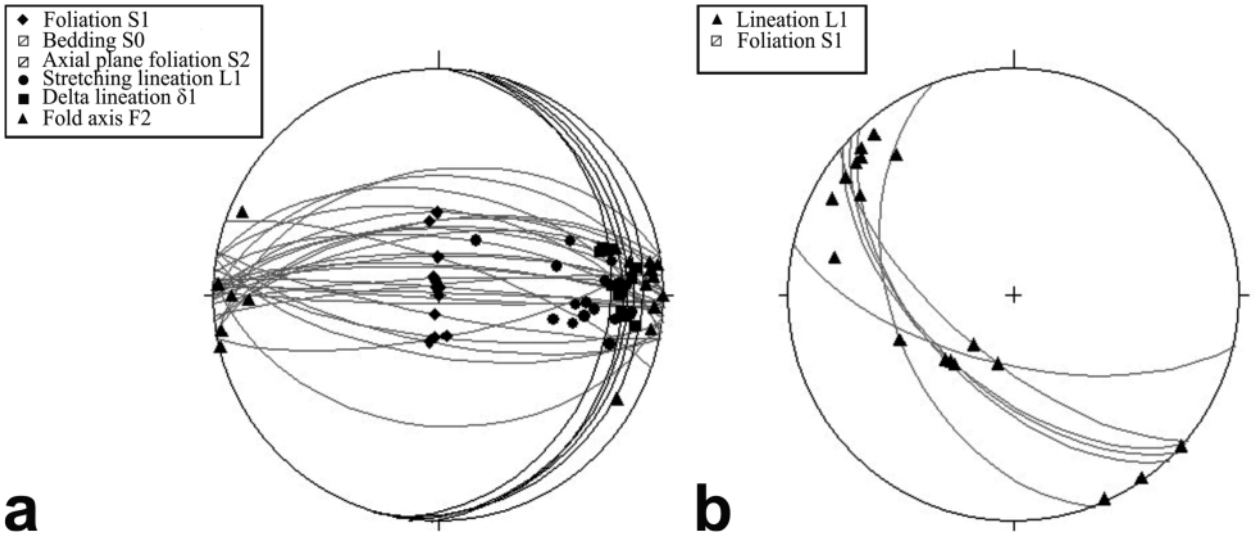

Figure 6: Orientation data of structures exposed in level I. A - Foliation S1 subparallel to bedding S0, axial plane foliation S2, stretching lineation L1, delta lineation δ1, fold axis F2. For further explanation, see text. Lambert (Schmidt) projection, lower hemisphere. B - Foliation S1 and lineation L1 of the gypsum mylonite of levels VII and VIII. Lambert (Schmidt) projection, lower hemisphere.

The banded carbonate mylonite (Fig. 5a) is about 10 meter thick, strongly foliated and shows a centimetre-scale, here subvertical, banding respectively foliation. The uppermost 50 cm of the carbonate mylonite are rich in pyrite, and show evidence of an axial plane foliation. The banded mylonites are folded with subhorizontal fold axes, here described as fold axes F_{3b}, and a cogenetic fracture cleavage (Fig. 5e), here tentatively assigned to S_{3b} (Fig. 6a) of the deformation stage D_{3b} established below.

The strongly foliated fine-grained anhydrite and carbonate mylonite is preserved with a WNW-trending, subhorizontal stretching lineation (Fig. 6a) together constituting an L-S fabric. This indicates emplacement of the Haselgebirge evaporite mélange under ductile conditions. Based on fluid inclusion studies on anhydrite and K-feldspar, Spötl et al. (1996) and Wiesheu (1997) found a maximum temperature of > 240°C for rocks in the Moosegg quarry, which make ductile conditions reasonable. Furthermore, E-W trending folds are associated with the steeply dipping axial plane foliation and indicate N-S shortening.

Three different types of shear sense criteria of the shear fabric composed of foliation S_1 and L_1 have been found in thin sections of carbonate and anhydrite mylonites oriented perpendicular to the foliation S_1 and parallel to the stretching lineation L_1 (Fig. 7). They include: (1) Thin section AS-I-D (S_1 010/61), an anhydrite mylonite, shows an oblique orientation of elongated, subparallel anhydrite grains (Fig. 7d), which have been formed throughout recrystallization of anhydrite. The fabric indicates a shear top-to-the-west displacement of the overlying rocks. (2) Thin section AS-I-E (S_0=S_1 006/79) includes an asymmetric isoclinal intrafolial fold with long and short fold limbs (Fig. 7a and b). The vergency indicates a top W movement of the hangingwall unit. (3) Some of the anhydrite and carbonate mylonites show rigid pyrite grains with asymmetric pressure fringes. Especially the asymmetric grains in thin section AS-I-C indicate a top-west movement (Fig. 7c).

The ductile Haselgebirge thrust fault is also exposed in the eastern parts of levels VII and VIII (Figs. 3, 8) The gypsum crystals are ca. millimetre-sized, and we tentatively assume that the gypsum crystals formed by secondary transformation from anhydrite. In the gypsum mylonite and in some remnants at the base of the overlying gypsum breccia, the foliation S_1

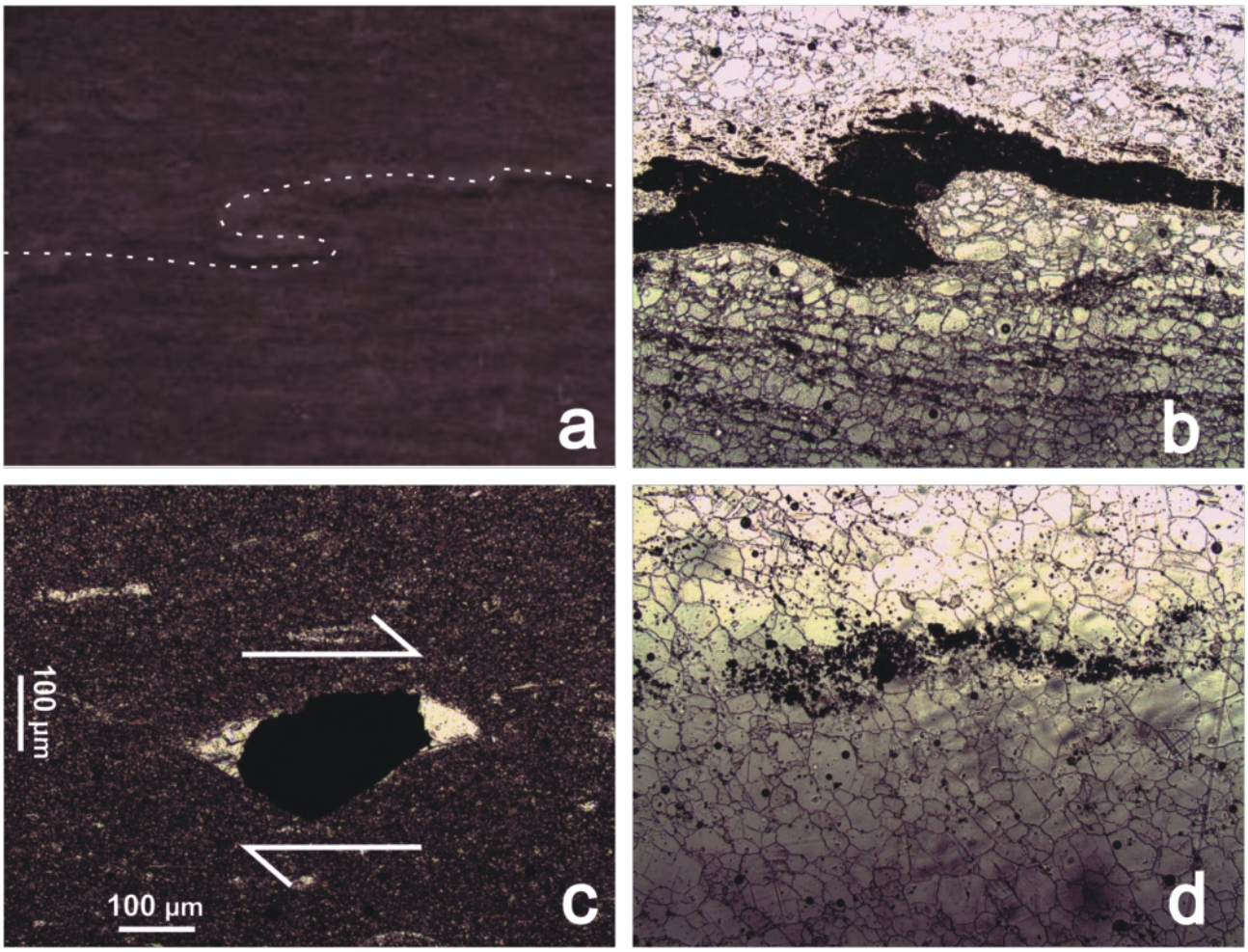

Figure 7: Examples of shear criteria showing top W motion. a – Thin section-scale isoclinal intrafolial fold (scan of a thin section). Long edge of the photomicrograph corresponds to (~ 40 millimeter). b – Microphotograph showing an isoclinal intrafolial fold. c - Asymmetric pressure fringes indicating a top west movement. d - Microphotograph showing oblique orientation of subparallel anhydrite grains in respect to elongated subhorizontal aggregates of ore grains (sample AS-I-D; S_1 010/61).

and lineation L_1 vary in orientation and dip steeply to the W or WSW or even S, respectively (Fig. 6b). No shear sense could be deduced because of secondary recrystallization throughout.

5.3 Description of other structures of Moosegg quarry

In the other levels of the Moosegg quarry, ductile and brittle structures also occur. The direction of movement can be derived from asymmetric dolomite clasts (Fig. 9a) in foliated gypsum and from well preserved slickensides (Fig. 9b). Beside foliation, ductile structures including some large- and small-scaled shear bands and mainly small folds are also visible.

Most of the gypsum breccias contain foliated and stretched gypsum components (Fig. 4c). Compared with the matrix, the components of the foliated dark gypsum breccia of level V (Fig. 4l) show in part a differently orientated foliation indicating a secondary overprint and therefore several stages of deformation.

Several dark shear bands within gypsum in the central parts of level IV and V (Fig. 4j) are part of a ductile shear zone and show a normal fault with a W-down-movement of the hanging-wall. These shear bands are composed of dark, strongly foliated and weathered gypsum and clayey fault gouges. Furthermore, red gypsum and red anhydrite with trace amounts of langbeinite (Fig. 3) are quite commonly associated with these shear bands.

The Moosegg quarry also exhibits cataclastically deformed black dolomite boudins within foliated anhydrite and gypsum extension joints (Fig. 5f). Hydraulic breccias (Fig. 4k) crop out in the south-eastern parts of levels IV and VII. The fluid-assisted brecciation postdates ductile deformation of sulphates. The origin of the water could be explained by conversion of gypsum to anhydrite (temperatures between 60 and 125°C).

The obtained new kinematic data is displayed in a structural map together with the different deformation stages (see chapter 5.4. and Fig. 3). The foliation data (Fig. 10a) represents a N-S-trending maximum accompanied by open wide folds. Lineation data (Fig. 10b) of Moosegg shows three different maxima, E–W, NW–SE- and SW-trending. The latter one shows a large scatter and is possibly related to folding.

Fold axis data (Fig. 10c) displays dominant E–W trending folds with subhorizontal fold axes and indicates N-S-compression. Subordinate N-S-trending folds also occur. Extension joint data (Fig. 10d) features two dominant joint directions. The N-S-trending joints constitute ac-joints and the E-W trending ones bc-joints to the dominant E–W-trending folds.

5.4 Chronology of deformation stages

In the following, we set up the succession of deformation events. The succession is based on three sources of data: (1) the re-evaluation of the map-scale structures of the geological map (Fig. 2a) (Plöchinger, 1987), combined with our own observations, (2) the succession of outcrop-scale deformation structures and their kinematics as we found it in the field, and (3) the succession of brittle deformation structures of the central and eastern NCA published by Peresson and Decker (1997a, b). The publications of Peresson and Decker (1997a, b) also yield absolute age constraints, which are not available from the working area solely due to the absence of post-lowermost Cretaceous sedimentary units.

In this chapter, the fault slip data, which constrain the evolution of the paleostress fields within the Haselgebirge evaporite mélange and surrounding geological units, is also presented. For details of the methodology of the paleostress technique, see the Appendix. For the reconstruction of the succession of deformation events within the particular sector of the NCA, we collected data at 40 stations all over the investigated area (for details, see below).

The paleostress analysis of faults shows ten different deformations stages from late Early Cretaceous to post-Miocene. The results, ordered in a succession from oldest to youngest, are compiled in Table 1 and are graphically shown in Figures 11 and 12. The results of deformation stages from the Moosegg quarry are shown in Table 2 and Figure 13. The relative succession of paleostress tensor groups was deduced from

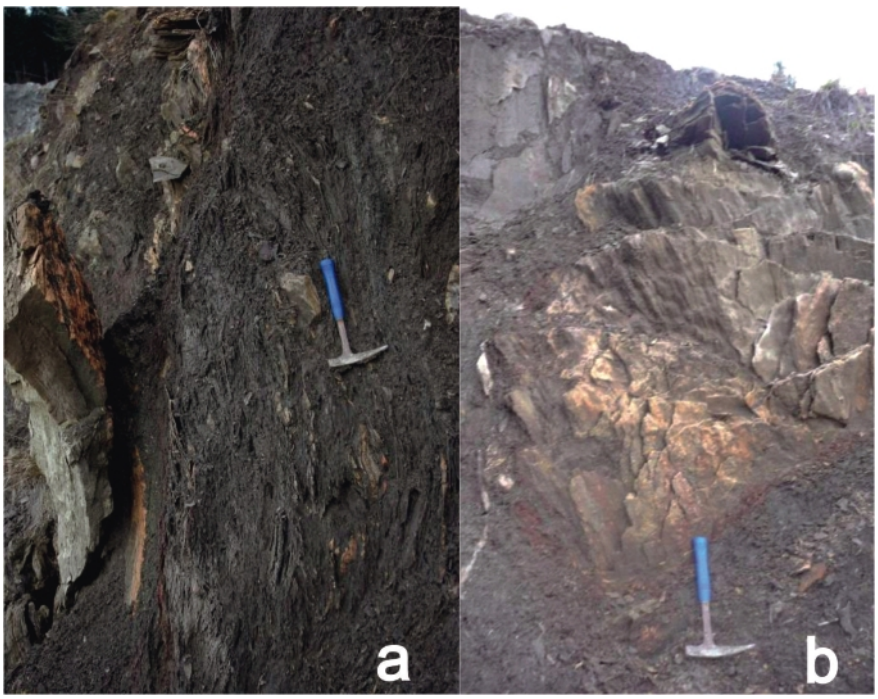

Figure 8: a, b - Gypsum mylonites of level VII and VIII. a – Gypsum mylonite on left side in contact with dark sheared shale. b - Note steeply plunging stretching lineation.

No	Location	Coordinates (Google Earth)	Lithology	Age	Stress regime	Event	Method applied	s 1	s 2	s 3	R
3	Moosegg Quarry	7°36'59.84"N 13°13'14.80"E	Gypsum mylonite	late Early Cretaceous - early Late Cretaceous	Thrust fault	D 1					
5	Moosegg Quarry	47°36'54.00"N 13°13'1.01"E	Banded anhydrite-carbonate mylonite	late Early Cretaceous - early Late Cretaceous	Thrust fault	D 1					
22	Kertererbach gorge	47°36'58.25"N 13°11'44.40"E	Oberalm Formation	? older than Late Eocene	Strike-slip fault	D 1	NDA	287 / 10	073 / 78	196 / 07	0.41
22	Kertererbach gorge	47°36'58.25"N 3°11'44.40"E	Oberalm Formation	? older than Late Eocene	Strike-slip fault	D 2	NDA	247 / 04	351 / 74	156 / 15	0.51
1	Moosegg Quarry	47°37'2.45"N 13°13'15.43"E	Light strongly foliated gypsum	Late Eocene - ?Oligocene	Normal Fault	D 3a	NDA	276 / 65	142 / 18	046 / 17	0.51
2	Moosegg Quarry	47°37'1.54"N 13°13'9.24"E	Light massive gypsum	Late Eocene - ?Oligocene	Strike-slip fault	D 3a	NDA	142 / 24	266 / 51	038 / 29	0.48
25	Kertererbach gorge	47°37'6.41"N 13°12'14.15"E	Schrambach Formation, sandy marl (Upper Rossfeld Fm.)	Late Eocene - ?Oligocene	Reverse Fault	D 3a	NDA	309 / 05	218 / 10	065 / 78	0.56
36	Schönleiten	47°37'13.36"N 13°14'11.59"E	Thin-bedded chert-bearing sandy marl (Upper Hauterivian), Upper Rossfeld Fm.	Late Eocene - ?Oligocene	Reverse Fault	D 3a	NDA	123 / 38	018 / 18	268 / 46	0.55
18	Strubau	7°37'24.68"N 13°11'10.58"E	Oberalm Formation	Oligocene? - Early/Middle Miocene	Strike-slip fault	D 3b	NDA	358 / 09	131 / 77	266 / 10	0.43
19	Strubau	7°37'17.63"N 13°10'38.16"E	Oberalm Formation	Oligocene? - Early/Middle Miocene	Strike-slip fault	D 3b	NDA	008 / 06	164 / 83	277 / 03	0.54
38	Seebach, base Schwarzer Berg	47°36'46.20"N 13°15'9.02"E	Rossfeld Formation to Ramsau Dolomite boundary	Oligocene? - Early/Middle Miocene	Strike-slip fault	D 3b	NDA	345 / 06	096 / 75	253 / 14	0.50
21	Kertererbach gorge	47°36'57.12"N 13°11'36.00"E	Oberalm Formation	? older than Middle Miocene	Grubach Normal fault	D 4	NDA	072 / 51	239 / 38	334 / 07	0.50
26	Grubach	47°37'8.91"N 3°12'19.38"E	Oberalm Formation	? older than Middle Miocene	Normal fault	D 4	NDA	039 / 61	242 / 27	147 / 10	0.46
3	Moosegg Quarry	47°36'59.84"N 3°13'14.80"E	Gypsum mylonite (thrust fault zone)	Middle Miocene	Reverse fault	D 5	NDA	247 / 37	353 / 20	106 / 46	0.49
4	Moosegg Quarry	47°36'59.51"N 13°13'9.63"E	Gypsum breccia with two types of dark components	Middle Miocene	Reverse fault	D 5	NDA	227 / 19	127 / 27	348 / 56	0.55
5	Moosegg Quarry	47°36'54.00"N 13°13'1.01"E	Banded anhydrite-carbonate mylonite	Middle Miocene	Strike-slip fault	D 5	NDA	028 / 14	255 / 70	122 / 14	0.48
18	Strubau	47°37'24.68"N 3°11'10.58"E	Oberalm Formation	Middle Miocene	Strike-slip fault	D 5	NDA	062 / 18	227 / 71	330 / 05	0.50
22	Kertererbach gorge	47°36'58.25"N 13°11'44.40"E	Oberalm Formation (pull apart)	Middle Miocene	Strike-slip fault	D 5	NDA	030 / 38	188 / 50	292 / 11	0.60
22	Kertererbach gorge	47°36'58.25"N 13°11'44.40"E	Oberalm Formation (cataclastic shear zone)	Middle Miocene	Strike-slip fault	D 5	NDA	062 / 22	180 / 49	317 / 32	0.39
23	Kertererbach gorge	47°37'2.36"N 13°12'1.94"E	Schrambach Formation (cataclastic shear zone) or siliceous, sandy limestone (Hochreith Formation), Lower Rossfeld Formation	Middle Miocene	Strike-slip fault	D 5	NDA	046 / 26	200 / 61	311 / 11	0.48
24	Kertererbach gorge	47°37'5.24"N 13°12'7.90"E	Oberalm Formation (cataclastic shear zone)	Middle Miocene	Strike-slip fault	D 5	NDA	037 / 37	231 / 52	132 / 07	0.53
25	Kertererbach gorge	47°37'6.41"N 13°12'14.15"E	Schrambach Formation or sandy marl	Middle Miocene	Strike-slip fault	D 5	NDA	225 / 19	342 / 54	124 / 29	0.56
25	Kertererbach gorge	47°37'6.41"N 13°12'14.15"E	Schrambach Formation or sandy marl	Middle Miocene	Reverse fault	D 5	NDA	198 / 29	291 / 04	028 / 61	0.52
26	Grubach	47°37'8.91"N 13°12'19.38"E	Oberalm Formation	Middle Miocene	Strike-slip fault	D 5	NDA	226 / 05	097 / 82	317 / 06	0.50
31	Hochreith	47°36'20.15"N 13°12'0.40"E	Siliceous, sandy limestone (Hochreith Formation), Lower Rossfeld Formation	Middle Miocene	Reverse fault	D 5	NDA	039 / 36	143 / 19	255 / 47	0.50
33	Krautegg	47°37'19.33"N 3°13'20.95"E	Bedded Dachstein Limestone	Middle Miocene	Strike-slip fault	D 5	NDA	055 / 25	212 / 63	321 / 09	0.48
35	Schönleiten	47°37'14.76"N 13°14'6.81"E	Thin-stratified chert-bearing sandy marl (Upper Hauterivian) of Upper Rossfeld Fm.	Middle Miocene	Strike-slip fault	D 5	NDA	225 / 09	124 / 51	322 / 38	0.45
6	Schönleiten	47°37'13.36"N 13°14'11.59"E	Thin-stratified chert-bearing sandy marl (Upper Hauterivian) of Upper Rossfeld Fm.	Middle Miocene	Strike-slip fault	D 5	NDA	039 / 17	142 / 36	289 / 49	0.48
6	Moosegg Quarry	47°37'2.10"N 13°13'8.63"E	Shear bands within dark gypsum breccia	Middle Miocene	Normal fault	D 6	NDA	178 / 76	326 / 12	057 / 07	0.46
7	Moosegg Quarry	47°36'59.34"N 13°13'7.94"E	Gypsum breccia with two types of dark componentes	Middle Miocene	Normal fault	D 6	NDA	107 / 40	009 / 09	268 / 48	0.50

Table 1: Coordinates, lithology, assumed age and paleostress data of deformation events in the surroundings of the Moosegg quarry. Locations can be found in Figures 2a and 11-13. Abbreviations: σ_1, σ_2, σ_3, orientation of maximum, intermediate and minimum principal stress axes; NDA, numerical dynamical analysis; R, shape factor of the paleostress tensor.

No	Location	Coordinates (Google Earth)	Lithology	Age	Stress regime	Event	Method applied	s 1	s 2	s 3	R
8	Moosegg Quarry	47°36'55.32"N 13°12'56.80"E	Gypsum breccia	Middle Miocene	Normal fault	D 6	NDA	101 / 70	202 / 04	293 / 20	0.50
9	Moosegg Quarry	47°36'59.31"N 13°13'2.35"E	Light-colored massive gypsum	Late Miocene (Pannonian)	Normal fault	D 6	NDA	247 / 56	040 / 31	138 / 13	0.55
27	Stallerhof	47°36'28.99"N 13°11'34.20"E	Sandy marl, hornblende-carrying quartz-sandstone (Upper Valanginian - Lower Hauterivian), Lower Rossfeld Formation	Middle Miocene	Normal fault	D 6	NDA	294 / 33	027 / 04	123 / 56	0.55
29	Hochreith	47°36'42.47"N 13°11'48.80"E	Siliceous, sandy limestone (Hochreith Formation), Lower Rossfeld Formation	Middle Miocene	Normal fault	D 6	NDA	013 / 38	192 / 52	283 / 00	0.50
31	Hochreith	7°36'20.15"N 13°12'0.40"E	Siliceous, sandy limestone (Hochreith Formation), Lower Rossfeld Formation	Middle Miocene	Normal fault	D 6	NDA	138 / 58	330 / 31	237 / 05	0.50
36	Schönleiten	47°37'13.36"N 13°14'11.59"E	Thin-stratified chert-carrying sandy marl (Upper Hauterivian) Upper Rossfeld Fm.	Middle Miocene	Normal fault	D 6	NDA	172 / 83	344 / 07	074 / 01	0.49
10	Moosegg Quarry	47°37'0.77"N 13°13'3.53"E	Dark gypsum breccia	Late Miocene (Pannonian)	Normal fault	D 7	NDA	104 / 37	216 / 26	332 / 42	0.49
11	Moosegg Quarry	7°36'58.61"N 13°13'7.59"E	Gypsum breccia with two types of dark components	Late Miocene (Pannonian)	Strike-slip fault	D 7	NDA	110/01	201/50	19/40	0.51
12	Moosegg Quarry	47°37'2.07"N 13°13'6.57"E	Dark gypsum breccia	Late Miocene (Pannonian)	Strike-slip fault	D 7	NDA	074 / 25	221 / 60	337 / 14	0.49
13	Moosegg Quarry	7°36'59.96"N 13°13'9.12"E	Gypsum breccia with two types of dark components	Late Miocene (Pannonian)	Strike-slip fault	D 7	NDA	087 / 12	212 / 70	354 / 16	0.50
14	Moosegg Quarry	47°37'2.03"N 3°13'10.83"E	Light massive gypsum/lenses of anhydrite	Late Miocene (Pannonian)	Strike-slip fault	D 7	NDA	094 / 19	252 / 70	002 / 07	0.50
15	Moosegg Quarry	47°37'1.79"N 13°13'14.20"E	Light strongly foliated gypsum	Late Miocene (Pannonian)	Strike-slip fault	D 7	NDA	291 / 03	047 / 83	201 / 06	0.50
19	Strubau	7°37'17.63"N 3°10'38.16"E	Oberalm Formation	Late Miocene (Pannonian)	Strike-slip fault	D 7	NDA	103 / 03	229 / 86	013 / 04	0.49
22	Kertererbach gorge	47°36'58.25"N 13°11'44.40"E	Oberalm Formation	Late Miocene (Pannonian)	Strike-slip fault	D 7	NDA	104 / 04	284 / 86	194 / 00	0.42
26	Grubach	47°37'8.91"N 13°12'19.38"E	Oberalm Formation	Late Miocene (Pannonian)	Strike-slip fault	D 7	NDA	274 / 19	088 / 71	183 / 02	0.48
28	Stallerhof	47°36'29.95"N 13°11'38.81"E	Sandy marl, hornblende-bearing quartz-sandstone (Upper Valanginian - Lower Hauterivian), Lower Rossfeld Formation	Late Miocene (Pannonian)	Reverse fault	D 7	NDA	111 / 01	202 / 47	020 / 42	0.49
30	Hochreith	7°36'32.82"N 3°11'52.75"E	Siliceous sandy limestone (Hochreith Formation), Lower Rossfeld Formation	Late Miocene (Pannonian)	Reverse fault	D 7	NDA	088 / 32	351 / 12	242 / 56	0.44
32	base Schwarzer Berg	7°36'48.02"N 13°13'57.82"E	Wetterstein Dolomite	Late Miocene (Pannonian)	Reverse fault	D 7	NDA	251 / 16	159 / 05	054 / 73	0.20
34	Krautegg	47°37'28.20"N 13°13'37.22"E	Siliceous, sandy Limestone (Hochreith Formation), Lower Rossfeld Formation	Late Miocene (Pannonian)	Strike-slip fault	D 7	NDA	254 / 19	137 / 53	356 / 31	0.52
35	Schönleiten	7°37'14.76"N 13°14'6.81"E	Thin-bedded chert-bearing sandy marl (Upper Hauterivian) of Upper Rossfeld Formation	Late Miocene (Pannonian)	Strike-slip fault	D 7	NDA	256 / 02	163 / 61	347 / 29	0.52
37	Seebach submontane Schwarzer Berg	47°36'53.51"N 13°15'13.38"E	Sandy marl, hornblende-bearing quartz-sandstone (Upper Valanginian - Lower Hauterivian), Lower Rossfeld Formation	Late Miocene (Pannonian)	Strike-slip fault	D 7	NDA	106 / 06	002 / 65	199 / 24	0.52
38	Seebach, base Schwarzer Berg	47°36'46.75"N 13°15'5.49"E	Rossfeld Formation - Ramsau Dolomite boundary	Late Miocene (Pannonian)	Strike-slip fault	D 7	NDA	077 / 08	271 / 82	167 / 02	0.53
39	Seebach, base Schwarzer Berg	47°36'46.75"N 13°15'5.49"E	Ramsau Dolomite	Late Miocene (Pannonian)	Strike-slip fault	D 7	NDA	275 / 10	053 / 77	184 / 09	0.51
40	Wegscheid	47°38'8.38"N 13°12'12.58"E	Schrambach Formation	Late Miocene (Pannonian)	Strike-slip fault	D 7	NDA	071 / 21	216 / 65	336 / 13	0.49
16	Moosegg quarry	47°37'4.63"N 3°13'10.37"E	Dark strongly foliated gypsum breccia	Late - post-Miocene	Normal fault	D 8	NDA	083 / 63	294 / 24	199 / 12	0.49
17	Moosegg quarry	47°37'3.40"N 3°13'14.72"E	Dark strongly foliated gypsum breccia	Late - post-Miocene	Normal fault	D 8	NDA	089 / 72	239 / 16	332 / 09	0.50
20	Kertererbach gorge	7°36'56.09"N 3°11'22.63"E	Oberalm Formation	Late - post-Miocene	Normal fault	D 8	NDA	278 / 77	089 / 13	180 / 02	0.47
23	Kertererbach gorge	47°37'2.36"N 13°12'1.94"E	Schrambach Formation	Late - post-Miocene	Normal fault	D 8	NDA	014 / 51	271 / 11	173 / 37	0.54
31	Hochreith	47°36'20.15"N 13°12'0.40"E	Siliceous, sandy Limestone (Hochteith Formation) Lower Rossfeld Formation	Late - post-Miocene	Normal fault	D 8	NDA	212 / 57	072 / 27	332 / 18	0.55
35	Schönleiten	47°37'14.76"N 13°14'6.81"E	Thin-stratified chert-bearing sandy marl (Upper Hauterivian) Upper Rossfeld Formation	Late - post-Miocene	Normal fault	D 8	NDA	295 / 72	082 / 15	174 / 09	0.73

Table 1 continue

overprinting relationships in the key outcrops of Kertererbach gorge and Moosegg quarry.

Starting with deformation stage D_{3a}, we follow the event chronology from Peresson and Decker (1997a, b). In the entire area, the NE–SW strike-slip compression of deformation stage D_5 and E–W strike slip compression of deformation stage D_7 are predominant. Folds are mainly E–W trending and therefore represent the deformation stage D_{3b} (N-S-compression). In the Moosegg quarry, we also detected subordinate N–S trending folds (see above).

Deformation stage D_1, WNW-directed Haselgebirge thrust fault (Fig. 6a and b). Over a period from late Early Cretaceous to possibly early Late Cretaceous, the Lower Juvavic Haselgebirge nappe was thrusted over the Lower Cretaceous Rossfeld Formation and the Lower Aptian Grabenwald Formation. At the base of the Haselgebirge Fm., strongly foliated fine-grained anhydrite and carbonate mylonite is preserved with WNW-trending, subhorizontal stretching lineation (L-S fabric) indicating emplacement of the Haselgebirge evaporite mélange within ductile conditions (T > 240 °C). The age of this deformation event is younger than early Aptian, and we tentatively correlate this event with the main stage of nappe stacking within the NCA, predating Gosau Group deposition elsewhere within the NCA.

Locally, we found sinistral NW-SE trending strike-slip faults showing E-W compression and N-S-extension. This stage is not described further in this work, as it is only observed at station 22 (Figs. 11, 12) in the Kertererbach gorge (Fig. 2a) and may have been reactivated and overprinted by deformation stage D_7 (also E–W-compression). The exact age has to be discussed but an age older than Late Eocene is assured by overprint relationships to subsequent structures.

The NE–SW-trending dextral strike-slip F1 and 3 faults are observed in the map and have been measured mainly at station 22 in Kerterbach gorge (Fig. 2a). The paleostress tensor group of deformation stage D_2 shows NE–SW strike-slip compression including NW–SE extension. There is also the possibility of overprinting and reactivation by deformation stage D_5 (NE–SW-compression). Deformation stage D_2 is overprinted by D_{3a} and, therefore, has to be of an age older than Late Eocene.

Deformation stage D_{3a}, NW-SE-compression. This tensor group comprises NW–SE trending normal faults, steep N–S and E–W-trending reverse faults and N–S-trending sinistral

Figure 9: a - Boudinage and asymmetric clasts of dolomite in foliated gypsum. b - Well preserved slickensides of level IV. c, d - Grubach normal fault in outcrops. c - Grubach normal fault exposed in Kertererbach gorge. d - Road cut along the road from Wegscheid to Grubach.

No	Location	Coordinates	Lithology	Age	Stress regime	Event	Method applied	s 1	s 2	s 3	R
1	Moosegg Quarry	47°37'2.45"N 13°13'15.43"E	Light-colored strongly foliated gypsum	Late Eocene - ?Oligocene	Normal fault	D 3a	NDA	276 / 65	142 / 18	046 / 17	0.51
2	Moosegg Quarry	47°37'1.54"N 13°13'9.24"E	Light massive gypsum	Late Eocene - ?Oligocene	Strike-slip fault	D 3a	NDA	142 / 24	266 / 51	038 / 29	0.48
3	Moosegg Quarry	47°36'59.84"N 13°13'14.80"E	Gypsum mylonite (thrust fault zone)	Middle Miocene	Reverse fault	D 5	NDA	247 / 37	353 / 20	106 / 46	0.49
4	Moosegg Quarry	47°36'59.51"N 13°13'9.63"E	Gypsum breccia with two types of dark components	Middle Miocene	Reverse fault	D 5	NDA	227 / 19	127 / 27	348 / 56	0.55
5	Moosegg Quarry	47°36'54.00"N 13°13'1.01"E	Banded anhydrite/mylonitic limestone	Middle Miocene	Strike-slip fault	D 5	NDA	028 / 14	255 / 70	122 / 14	0.48
6	Moosegg Quarry	47°37'2.10"N 13°13'8.63"E	Shear bands within dark gypsum breccia	Middle Miocene	Normal fault	D 6	NDA	178 / 76	326 / 12	057 / 07	0.46
7	Moosegg Quarry	47°36'59.34"N 13°13'7.94"E	Gypsum breccia with two types of dark components	Middle Miocene	Normal fault	D 6	NDA	107 / 40	009 / 09	268 / 48	0.50
8	Moosegg Quarry	7°36'55.32"N 13°12'56.80"E	Gypsum breccia	Middle Miocene	Normal fault	D 6	NDA	101 / 70	202 / 04	293 / 20	0.50
9	Moosegg Quarry	47°36'59.31"N 13°13'2.35"E	Light-colored massive gypsum	Late Miocene (Pannonian)	Normal fault	D 6	NDA	247 / 56	040 / 31	138 / 13	0.55
10	Moosegg Quarry	47°37'0.77"N 13°13'3.53"E	Dark gypsum breccia	Late Miocene (Pannonian)	Normal fault	D 7	NDA	104 / 37	216 / 26	332 / 42	0.49
11	Moosegg Quarry	47°36'58.61"N 13°13'7.59"E	Gypsum breccia with two types of dark components	Late Miocene (Pannonian)	Strike-slip fault	D 7	NDA	110/01	201/50	19/40	0.51
12	Moosegg Quarry	47°37'2.07"N 13°13'6.57"E	Dark gypsum breccia	Late Miocene (Pannonian)	Strike-slip fault	D 7	NDA	074 / 25	221 / 60	337 / 14	0.49
13	Moosegg Quarry	7°36'59.96"N 13°13'9.12"E	Gypsum breccia with two types of dark components	Late Miocene (Pannonian)	Strike-slip fault	D 7	NDA	087 / 12	212 / 70	354 / 16	0.50
14	Moosegg Quarry	47°37'2.03"N 13°13'10.83"E	Light-colored massive gypsum with lenses of anhydrite	Late Miocene (Pannonian)	Strike-slip fault	D 7	NDA	094 / 19	252 / 70	002 / 07	0.50
15	Moosegg Quarry	47°37'1.79"N 13°13'14.20"E	Light strongly foliated gypsum	Late Miocene (Pannonian)	Strike-slip fault	D 7	NDA	291 / 03	047 / 83	201 / 06	0.50
16	Moosegg Quarry	47°37'4.63"N 13°13'10.37"E	Dark strongly foliated gypsum breccia	Late - post-Miocene	Normal fault	D 8	NDA	083 / 63	294 / 24	199 / 12	0.49
17	Moosegg Quarry	47°37'3.40"N 13°13'14.72"E	Dark strongly foliated gypsum breccia	Late - post-Miocene	Normal fault	D 8	NDA	089 / 72	239 / 16	332 / 09	0.50

Table 2: Coordinates, lithology, assumed age and paleostress data of deformation events in the Moosegg quarry. Locations can be found in Figures 2a and 13. Abbreviations: σ_1, σ_2, σ_3, orientation of maximum, intermediate and minimum principal stress axes; NDA, numerical dynamical analysis; R, shape factor of the paleostress tensor.

strike slip faults together constituting NW–SE compression (Fig. 13). By correlation with the succession proposed by Peresson and Decker (1997a, b) this deformation stage took place between Late Eocene and ?Oligocene.

Deformation stage D_{3b}, N–S compression and thrusting of the Schwarzer Berg Unit (Fig. 11a). In outcrops, we found NNE-trending sinistral strike-slip faults and NNW-trending dextral faults together constituting N–S strike-slip compression (Fig. 11a). This paleostress tensor group was formed from Oligocene(?) to Early-Middle Miocene according to Peresson and Decker (1997a, b). We tentatively assign the thrust of the Schwarzer Berg unit as part of the Göll-Lammer Masse over both the Rossfeld Formation (Osterhorn unit of the Tirolic nappe complex) and the Haselgebirge Formation (Lower Juvavic nappe) to deformation stage D_{3b}. In the course of this tectonic movement, the underlying nappes were folded along E–W trending fold axes, which resulted in the present syncline containing the Moosegg-klippe in its core.

Deformation stage D_4, NW–SE transtension with a sinistral strike-slip component (Fig. 11a). The fourth deformation stage comprises an ENE-trending high-angle normal fault juxtaposing Haselgebirge to Upper Jurassic Oberalm Formation. The above mentioned Grubach normal fault shows NW-SE extension with a sinistral strike-slip component (Fig. 9c, d). It can be traced across the whole study area in the Oberalm Formation from Strubau over Grubach (Fig. 2a) and westward in the bedded Dachstein Reef Limestone along the Gitschenwand up to Trattberg. The apparent minimum vertical offset amounts to approximately 700 m. A second conjugated normal fault branch further north juxtaposes the Upper Triassic Kössen Formation to the Oberalm Formation and the Oberalm base conglomerate (Fig. 2a). The timing of deformation stage D_4 can be discussed, but it is assured that D_4 is older than deformation stage D_5 (Middle Miocene).

Deformation stage D_5, NE-SW compression (Fig. 11b): This paleostress tensor group could be detected all over the study area and was formed, after Peresson and Decker (1997a, b), in Middle Miocene. It is characterised by mainly NE–SW trending, sometimes N–S trending sinistral and dextral strike slip faults. Subordinate N–S, NW–SE and E–W trending reverse

faults occur. Even though we found evidence for two deformation stages, both showing NE–SW compression and resulting in a NW–SE trending reverse fault and a NNE–SSW-trending strike-slip fault at station 25 in the Kertererbach gorge, we combined both events in D_5. Furthermore, deformation stage D_5 has probably overprinted and reactivated structures of deformation stage D_2.

Deformation stage D_6, E–W extension (Fig. 11a): This paleostress tensor group mainly comprises roughly N–S trending, E- and W-dipping normal faults and corresponding slickensides and striations. Together, they constitute a paleostress tensor showing E-W extension. Peresson and Decker (1997a, b) also found this paleostress tensor and assign a Middle Miocene age.

Deformation stage D_7, E–W compression (Fig. 12a): In several outcrops, we observed NE-trending dextral and NW-trending sinistral strike-slip faults together constituting E–W strike-slip compression. N–S trending reverse faults occur subordinately. Peresson and Decker (1997a, b) also found this paleostress tensor and assign a Late Miocene (Pannonian) age. The deformation stage D_7 (i.e., W–E compressive principal stress) is the most common in the investigated area.

Deformation stage D_8, N–S extension (Fig. 12b) is represented by conjugated NW–SE, NE–SW- and E–W-trending reverse faults, all indicating N–S extension. According to Peresson and Decker (1997a, b) the youngest deformation stage took place from Late- to post-Miocene.

6. Discussion

6.1 Structures and kinematic evolution

The structures of the Haselgebirge Fm. exposed in the Moosegg klippe bear all the signs of a tectonic mélange, where many different rock types form tectonic blocks within a gypsum/anhydrite matrix. Some of these blocks can be found in the footwall unit but the dominant rock types including magmatic and metamorphic rocks and some sedimentary units are exotic. Therefore, we suggest that many of these blocks were incorporated during the final emplacement as a tectonic nappe (see also Kozur, 1991).

The thrusting of the Haselgebirge Fm. is preserved in two different lithologies and locations of the Moosegg quarry. As mentioned before in the description of the structural map, the fine-grained, nearly vertically dipping foliated and subsequently folded anhydrite mylonites and anhydrite carbonate mylonites of level I represent a WNW-trending stretching lineation and together constitute an L-S fabric. Mylonites of the ductile Haselgebirge thrust fault are also exposed in the eastern parts of the levels VII and VIII. Foliation and lineation preserved in the gypsum mylonites, probably formed by secondary transformation from anhydrite, and the overlying gypsum breccia of levels VII and VIII also dip steeply to the W, SW or S.

Ratschbacher (1986), Ratschbacher and Neubauer (1989) and Ratschbacher et al. (1989) report ductile fabrics within low- and medium-grade metamorphic units of the Austroalpine nappe complex and generally found an E–W and subordinately an ESE–WNW trending stretching lineation. In general, all the shear criteria suggest top-west motion of hangingwall units (Fig. 7). The reported structural data of the Moosegg quarry fits well to these previous observations from metamorphic areas lo-

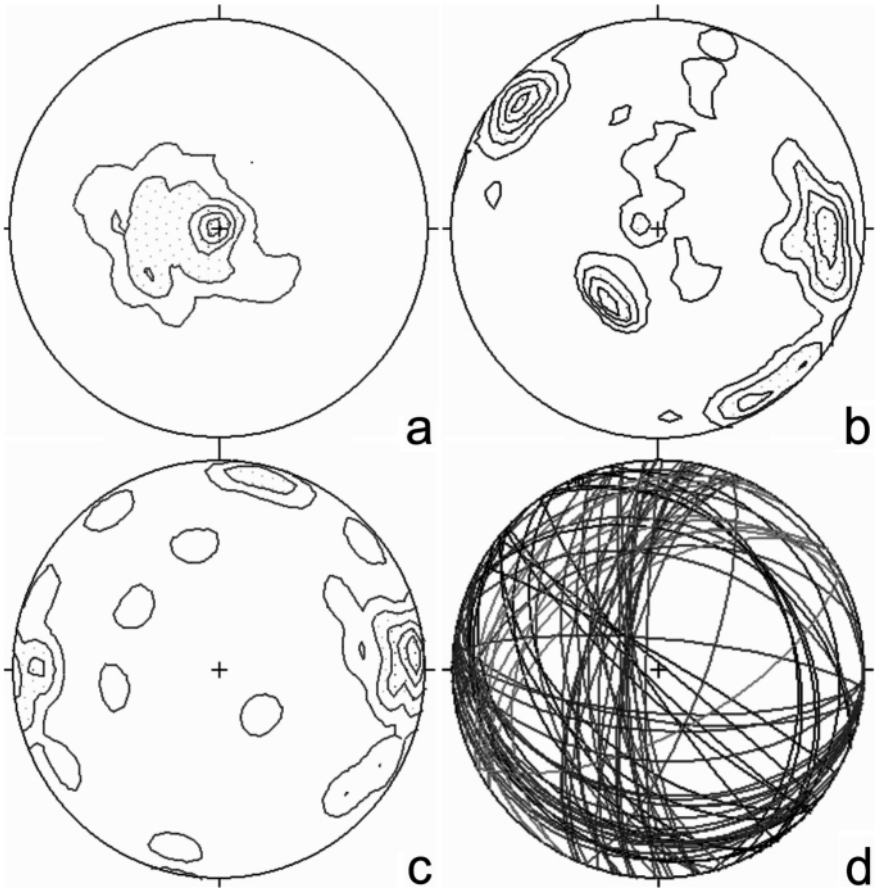

Figure 10: Orientation data of major structural elements of Haselgebirge exposed in the Moosegg quarry. a – Foliation data, 330 datasets, contours at 1.00, 3.00, 6.00, 9.00, 12.00. b - Lineation data, 166 datasets, contours at 1.00, 2.00, 3.00, 4.00, 5.00. c - Fold axes, 34 datasets, contours at 1.00, 3.00, 6.00, 9.00, 12.0. d - Extension joints of the entire Moosegg quarry, 106 datasets. Lambert (Schmidt) projections, lower hemisphere.

Figure 11: Paleostress data of various deformation stages: a - Deformation stages D_{3b}, D_4 and D_6. b - Deformation stage D_5. Abbrevi-ations: RF – Reverse Fault, SL – Strike slip fault, pa – pull apart, cs – cataclastic shear zone.

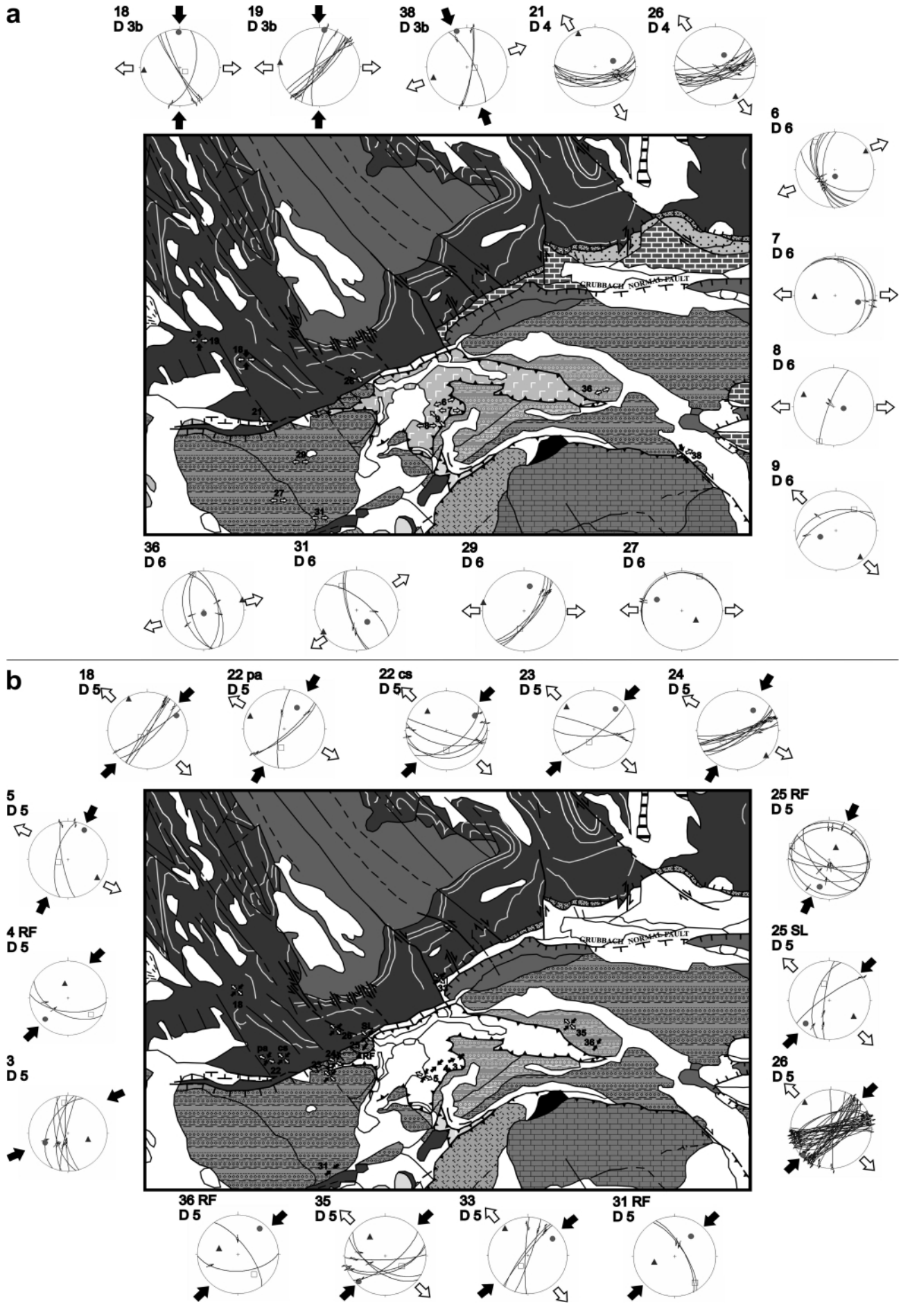
a
18
D 3b
19
D 3b
38
D 3b
21
D 4
26
D 4
6
D 6
7
D 6
8
D 6
9
D 6
GRUBBACH NORMAL FAULT
36
D 6
31
D 6
29
D 6
27
D 6
b
18
D 5
22 pa
D 5
22 cs
D 5
23
D 5
24
D 5
5
D 5
4 RF
D 5
3
D 5
25 RF
D 5
25 SL
D 5
26
D 5
GRUBBACH NORMAL FAULT
36 RF
D 5
35
D 5
33
D 5
31 RF
D 5

Location	Method	Temperature range (°C)	Temperature, best estimate (°C)	Author(s)
Northern Calcareous Alps	FI	270 - 360	315	Götzinger and Grum (1992)
Sazkammergut, Juvavic nappes	CAI	80 - > 350	80	Gawlick et al. (1994)
Moosegg	FI	220 - 260	240	Spötl et al. (1998b)
Moosegg	FI	> 300	300	Wiesheu (1997)
Moosegg	FI	300	300	Wiesheu (1997)
Lammer unit (Juvavic unit)	VR	max. 290	290	Rantitsch and Russegger (2005)

Table 3: Temperature conditions of eo-Alpine metamorphism within the Moosegg area, central Northern Calcareous Alps (from Leitner et al., 2011). For full sources, see cited manuscript. CAI, conodont colour alteration index, FI, fluid inclusions; VR, vitrinite reflectance.

cated much further south within lower structural units (e.g., Graywacke zone) of the Austroalpine nappe complex.

The anhydrite-carbonate mylonites are strongly foliated and the gypsum mylonites indicate an emplacement of the Hasel-gebirge evaporite mélange under ductile conditions formed at elevated temperatures consistent with previous temperature estimates (Table 3). In other places at the base of the Hasel-gebirge, anhydrite is transformed into foliated gypsum leaving behind a still well preserved L-S fabric, similar to the one encountered at level I of the Moosegg quarry. Furthermore, some large- and small-scaled gypsum shear bands, gypsum breccias with foliated gypsum clasts - some of which were again foliated and stretched - imply several stages of ductile deformation. Because of these peculiar fabrics, we interpret the formation of gypsum and anhydrite breccia as a result of fluid overpressure, possibly related in part to dehydration reactions of gypsum to anhydrite.

According to fluid inclusion studies and other methods (Table

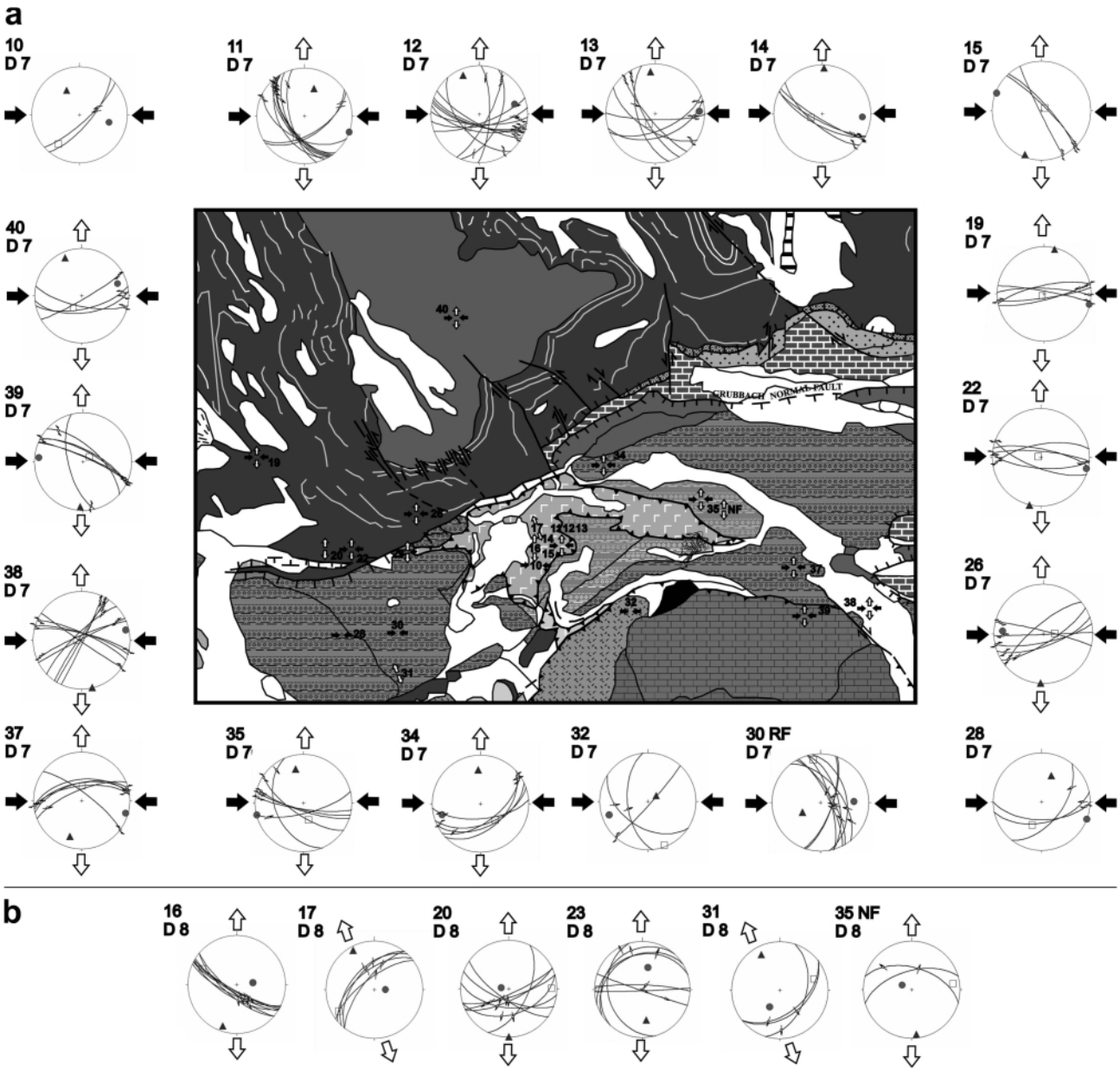

Figure 12: Paleostress data of a - Deformation stage D_7. and b – Deformation stage D_8 . Abbreviations: NF – Normal Fault.

3), the Haselgebirge sulphates experienced a relatively high temperature, >240°C (after Spötl et al., 1998b; Wiesheu, 1997). Fluid inclusion analyses on anhydrite samples of Berchtesgaden and Altaussee show similar results (see compilation in Leitner et al., 2011). We suggest that these fabrics formed in Early Cretaceous times, similar to other fabrics in the Central NCA. At Moosegg, Spötl et al. (1998a) found $^{40}Ar/^{39}Ar$ K-feldspar ages of around 145–154 Ma. We assume that these K-feldspars grew at static peak temperature conditions.

6.2 Dynamic interpretation of deformation stages

In the following, we discuss the geological significance of structures in a wider context (Fig. 15). Note, that we discuss orientations in the present-day coordinates being aware of rotations, which affected the Northern Calcareous Alps together with Austroalpine basement located further south (e.g., Pueyo et al., 2007 and references therein).

The WNW-directed thrust fault D_1 carried the Lower Juvavic Haselgebirge nappe over the Lower Cretaceous Rossfeld Formation and Grabenwald Formation. The age of this deformation event is younger than Aptian and we tentatively correlate this event to the main stage of nappe stacking within the NCA as well as with similarly old units in the Austroalpine exposed further to the south. There, ductile thrusts with similar kinematics dominate and the geochronological ages for thrust deformation range from ca. 110 to 80 Ma (e.g., Ratschbacher et al., 1989; Dallmeyer et al., 1998).

In the working area, deformation stage D_2, NE–SW strike-slip compression including NW–SE extension is constrained by map-scale brittle faults. We tentatively correlate these structures with such formed during initial stages of the development of Gosau basins on top of the NCA and Austroalpine basement nappe stacks (e.g., Neubauer et al., 1995; Wagreich and Decker, 2001). This implies a Late Cretaceous age of deformation event D_2.

Deformation stages D_{3a} and D_{3b}, NW–SE-compression and N–S compression are Late Eocene and Oligocene respecti-

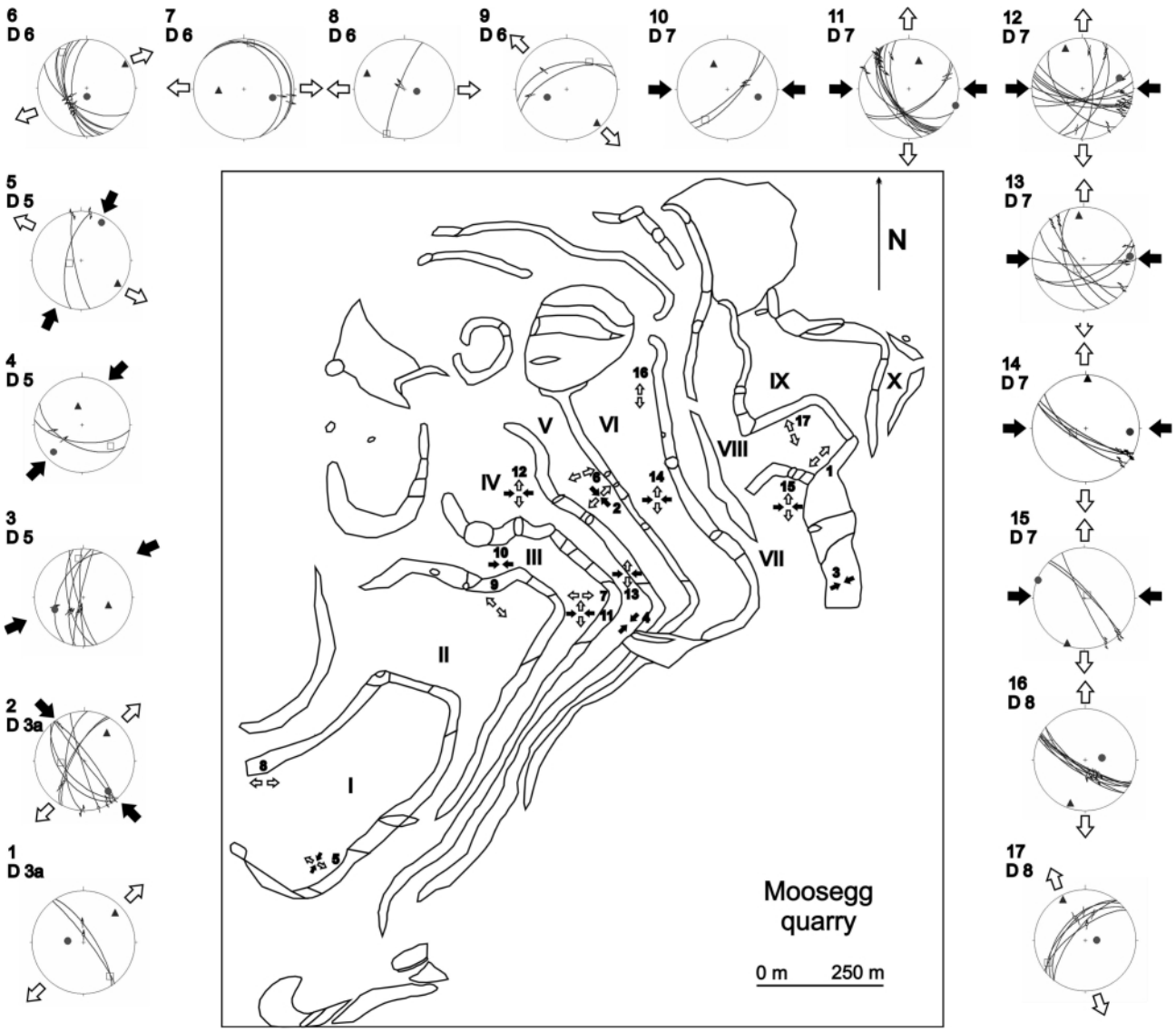

Figure 13: Paleostress data of various deformation stages in the Moosegg quarry.

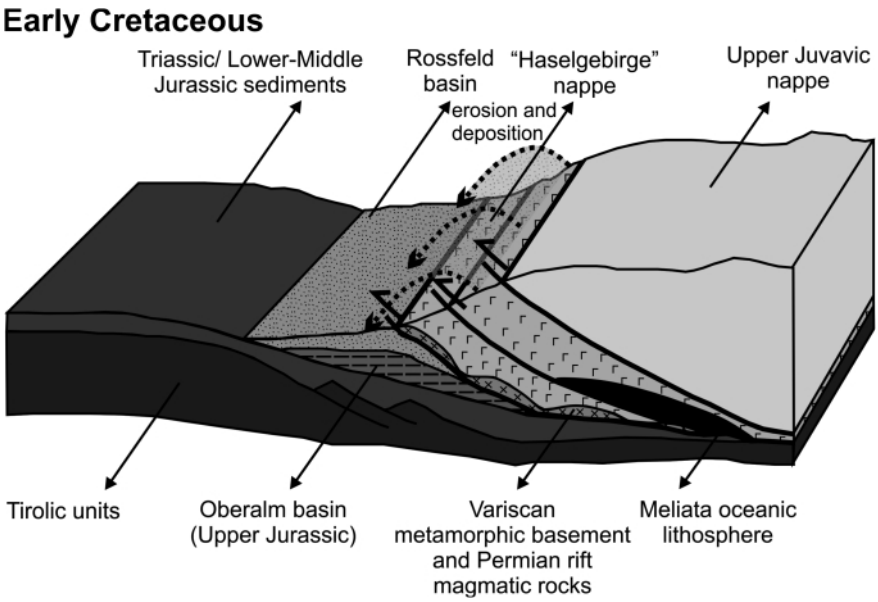

Figure 14: Tectonic model of the Cretaceous evolution of the Haselgebirge nappe.

vely Oligocene(?) to Early/Middle Miocene in age according to Peresson and Decker (1997a, b). This is a principal event of fault reactivation during emplacement of the NCA nappe stack over its footwall located in the north and subsequent further shortening. Note the gradual change of the shortening direction from NW–SE to N–S, which likely reflects a change of motion of the external driving force, the motion of the Adriatic microplate. In the working area, we tentatively assign the thrust of the Schwarzer Berg unit as part of the Göll-Lammer Masse over both the Rossfeld Formation (Osterhorn unit of the Tirolic nappe complex) and the Haselgebirge Formation (Lower Juvavic nappe) to deformation stage D_{3b}. During this tectonic movement, the underlying nappes were folded along E–W trending fold axes, which resulted in the present syncline comprising the Moosegg-klippe in its core. The NW-trending dextral strike-slip fault (F8 in Fig. 2a) cutting the Schwarzer Berg thrust fault and juxtaposing the Rossfeld Fm. to Ramsau Dolomite is also assigned to this event although it postdates thrusting.

In the working area, the prominent Grubach normal fault and similar faults further north show NW–SE extension with a sinistral strike-slip component (deformation stage D_4). This can be correlated with the main stage of lateral extrusion in the Eastern Alps (Ratschbacher et al., 1991), and similar sinistral transtensional structures can be found elsewhere in the Central Eastern Alps (e.g., Wang and Neubauer, 1998; Keil and Neubauer, 2011). Subsequent NE–SW compression (deformation stage D_5) relates this event with the main stage of east-directed lateral extrusion of the central Eastern Alps (Ratschbacher et al., 1989, 1991) in Middle Miocene times.

Subsequent ca. E–W extension (deformation stage D_6) was found over wide areas both in the NCA and southern adjacent areas of the Eastern Alps. E–W extension is also a consequence of east-directed lateral extrusion, and can be related to the activity of ESE-directed ductile low-angle normal faults at the eastern margin of the Tauern window and extension within the Styrian and Pannnonian basins (e.g., Genser and Neubauer, 1989; Sachsenhofer et al., 1997). In the NCA, Peresson and Decker (1997a, b) assign a Middle Miocene age to this event but it may have started earlier, during Early Miocene, along the central axis of the Eastern Alps. From the kinematic point of view, the E–W extension is triggered by previous NE-SW strike-slip compression and represents a continuum. However, on an outcrop scale, E–W extension can be clearly separated from previous NE–SW compression.

Peresson and Decker (1997a, b) noted the prominent E–W compression (our deformation stage D_7) for the first time and assigned to it a Late Miocene (Pannonian) age. This event reactivated many major ca. ENE-striking previously sinistral faults as dextral strike-slip faults. This event is explained by collision of the Carpathian arc with the East European foreland and backwards propagating stresses towards the Alps (Peresson and Decker (1997a, b). From a structural point of view, this event can be separated from the last event, N–S extension (deformation stage D_8), recorded in the working area, which indicates no E–W maximum compressive stresses. A Late-to post-Miocene to Pliocene age is assumed (Peresson and Decker, 1997a, b) and the extensional stresses may reflect gravity-driven orogenic collapse towards respective forelands after releasing compressional forces.

Together, all this kinematic data shows that this small segment of the central NCA reflects nearly all major large-scale processes that affected the Eastern Alps since late Early Cretaceous. Consequently, local structural data from a high structural level within an orogen can be taken to monitor nearly the complete succession of kinematic stages affecting the entire orogen.

7. Conclusions

Our results contribute to a reinterpretation of the emplacement of the Juvavic units (Fig. 14). In former studies the Juvavic nappe was considered to have resulted from gravity tectonics and the units were considered to have moved/been emplaced by gravity sliding (for example Gawlick and Lein., 2000; Missoni and Gawlick, 2011 and references therein). The ductile structures of the Moosegg quarry definitely disprove these models: According to our new data, the Haselgebirge bearing nappe was transported over the Lower Cretaceous Rossfeld Formation, which includes many clasts derived from the Haselgebirge Fm. and its exotic blocks were deposited in front of the incoming nappe (Fig. 14). Schorn et al. (submitted) demonstrated similarly aged Variscan white mica (349 ±

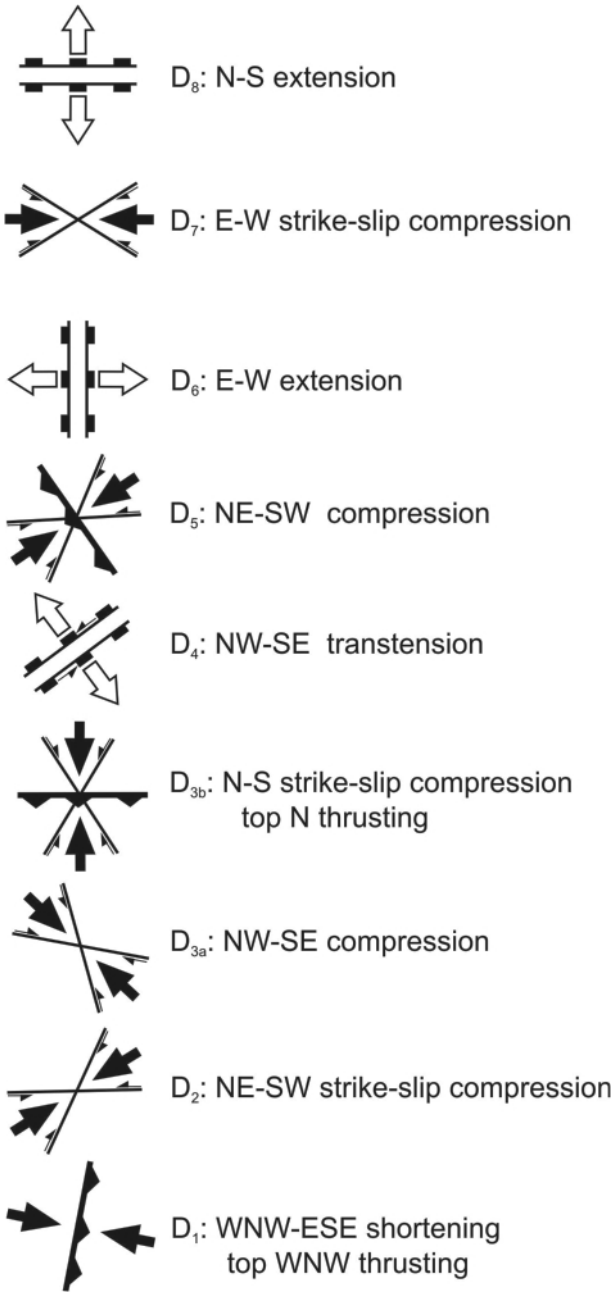

Figure 15: Scheme of kinematic evolution of the central Northern Calcareous Alps deduced from structural data of the Moosegg area. Orientations of kinematic data are given within present-day coordinates.

15 Ma, ~ 378 Ma) from metamorphic clasts of the Grubach klippe as von Eynatten et al. (1996) described from detrital white mica of the Rossfeld Formation (~ 320 – 360 Ma). The mylonitic fabrics at the base of the Haselgebirge klippe of Mossegg indicate formation during relatively high temperature conditions. Such mylonitic high-temperature shear zones were mapped in several other areas from the southern margin (e.g. Rettenstein and Werfen Imbricate zone) and close to the northern margin of the NCA (Berchtesgaden – Dürrnberg). With our study, we introduce a new tectonic interpretation of the investigated area, including a number of deformation stages, which reflects the structural and geological evolution of the NCA as a whole.

Acknowledgements

We thank to the Moldan Comp. for access to the Moosegg quarry. We gratefully acknowledge detailed reviews by Harry Fritz and Wolfgang E. Schollnberger and remarks and encouragement by the editor, Michael Wagreich, which helped clarify presentation and ideas. The initial pilot study was supported by the Stiftungs- und Förderungsgesellschaft der Universtät Salzburg. The work has been completed within the Polyhalite project (grant no. P22,728) funded by the Austrian Science Fund (FWF). We acknowledge improvement of the English of an earlier and the final versions of the manuscript by Isabella Merschdorf.

References

Angelier, J. and Méchler, P., 1977. Sur une methode de recherche des contraintes principales également utilisable en tectonique et en seismologie: la methode de dièdres droits. Bulletin de Societé Geologié de France, (7) 19, 1309–1318.

Angelier, J., 1979. Determination of the mean principal directions of stresses for a given fault population. Tectonophysics 56, T17–T26.

Angelier, J., 1989. From orientation to magnitudes in Paleostress determination using fault slip data. Journal of Structural Geology, 11, 37–50.

Armijo, R., Carey, E. and Cisternas, A. 1982. The inverse problem in microtectonics and the separation of tectonic phases. Tectonophysics, 82, 145–160.

Butler, R.W.H. and Paton, D. A., 2011. Evaluating lateral compaction in deepwater fold and thrust belts: How much are we missing from “nature’s sandbox”? GSA Today, 20, 3, 4-10, doi: 10.1130/GSATG77A.1.

Dallmeyer, R.D., Handler, R., Neubauer, F. and Fritz, H., 1998. Sequence of thrusting within a thick-skinned tectonic wedge: Evidence from $^{40}Ar/^{39}Ar$ ages from the Austroalpine nappe complex of the Eastern Alps. Journal of Geology, 106: 71–86.

Dallmeyer, R.D., Neubauer, F., and Fritz, H., 2008. The Meliata suture in the Carpathians: Regional significance and implications for the evolution of high-pressure wedges within collisional orogens. In: Siegesmund, S., Fügenschuh, B. and Froitzheim, N. (Eds.) Tectonic Aspects of the Alpine-Dinaride-Carpathian System. Geological Society [London] Special Publications, 298, 101–115.

Decker, K., Meschede, M. and Ring, U., 1992. Fault slip analysis along the northern margin of the Eastern Alps (Molasse, Helvetic nappes, North and South Penninic flysch, and the Northern Calcareous Alps). Tectonophysics, 223, 291-312.

Faupl, P. and Tollmann, A., 1978. Die Roßfeldschichten: Ein Beispiel für Sedimentation im Bereich einer tektonisch aktiven Tiefseerinne aus der kalkalpinen Unterkreide. Geologische Rundschau, 68, 93-120.

Faupl, P. and Wagreich, M., 2000. Late Jurassic to Eocene paleogeography and geodynamic evolution of the Eastern Alps. Mitteilungen der Österreichischen Geologischen Gesellschaft, 92, 79–94.

Frank, W. and Schlager, W., 2006. Jurassic strike slip versus subduction in the Eastern Alps. International Journal of Earth Sciences, 95, 431–450.

Gamond, J.F., 1983. Displacement features associated with fault zones: a comparison between observed and experimental models. Journal of Structural Geology, 5, 33–45.

Gamond, J.F., 1987. Bridge structures as sense of displacement in brittle fault zones. Journal of Structural Geology, 9, 609–620.

Gawlick, H.-J. and Lein, R., 2000. Die Salzlagerstätte Hallein-Bad Dürrnberg. Exkursionsführer Sediment 2000. Mitteilungen der Gesellschaft der Geologie- und Bergbaustudenten in Österreich, 44, 263–280.

Genser, H. and Neubauer, F., 1989. Low angle normal faults at the eastern margin of the Tauern window (Eastern Alps). Mitteilungen der Österreichischen Geologischen Gesellschaft, 81 (1988), 233–243.

Hudec, M.R. and Jackson, M.P.A., 2006. Advance of allochthonous salt sheets in passive margins and orogens. AAPG Bulletin, 90, 1535–1564.

Keil, M. and Neubauer, F., 2011. The Miocene Enns Valley basin (Austria) and the North Enns Valley fault. Austrian Journal of Earth Sciences, 104, 49–65.

Kober, L. 1955. Bau und Entstehung der Alpen, Second Ed., 379 p., Deuticke, Vienna.

Kozur, H. 1991. The Evolution of the Meliata-Hallstatt ocean and its significance for the early evolution of the Eastern Alps and Western Carpathians. Palaeogeography Palaeoclimatology Palaeoecology, 87, 109–135.

Leitner, C., Neubauer, F., Urai. J. L. and Schoenherr, J., 2011. Structure and Evolution of a Rocksalt-Mudrock-Tectonite: the Haselgebirge in the Northern Calcareous Alps. Journal of Structural Geology, 33, 970–984.

Linzer, H.-G., Ratschbacher, L. and Frisch, W., 1995. Transpressional collision structures in the upper crust: the fold-thrust belt of the Northern Calcareous Alps. Tectonophysics, 242, 41-61.

Linzer, H.G., Moser, F., Nemes, F., Ratschbacher, L. and Sperner, B. 1997. Build-up and dismembering of the eastern Northern Calcareous Alps. Tectonophysics, 272, 97–124.

Linzer, H.G. Decker, K. Peresson, H., Dell´Mour, R. and Frisch, W., 2002. Balancing lateral orogenic float of the Eastern Alps. Tectonophysics, 354, 211–237.

Mandl, G.W., 1982. Jurassische Gleittektonik im Bereich der Hallstätter Zone zwischen Bad Ischl und Bad Aussee (Salzkammergut Österreich). Mitteilungen der Gesellschaft der Geologie- und Bergbaustudenten in Österreich, 28, 55–76.

Mandl, G.W., 2000. The Alpine Sector of the Tethyan shelf – Example of Triassic to Jurassic sedimentation and deformation from the Northern Calcareous. Mitteilungen der Österreichischen Geologischen Gesellschaft, 92, 61–77.

Marret, R. and Almendinger, R.W., 1990. Kinematic analysis of fault slip data. Journal of Structural Geology, 12, 596–612.

Missoni, S. and Gawlick, H.-J., 2011. Evidence for Jurassic subduction from the Northern Calcareous Alps (Berchtesgaden; Austroalpine, Germany). International Journal of Earth Sciences, 100, 1605-1631, DOI 10.1007/s00531-010-0552-z.

Murray, R. C., 1964. Origin and diagenesis of gypsum and anhydrite. Journal of Sedimentary Research, 34, 512–523.

Neubauer, F., Dallmeyer, R. D., Dunkl, I. and Schirnik, D. 1995. Late Cretaceous exhumation of the metamorphic Gleinalm dome, Eastern Alps: kinematics, cooling history and sedimentary response in a sinistral wrench corridor. Tectonophysics, 242, 79–89.

Neubauer, F., Genser, J. and Handler, R., 2000. The Eastern Alps: Result of a two-stage collision process. Mitteilungen der Österreichischen Geologischen Gesellschaft, 92(1999), 117– 134.

Ortner, H., Reiter, F. and Acs, P. 2002. Easy handling of tectonic data: the programs Tectonics VP for Mac and Tectonics FP for Windows. Computer and Geosciences 28, 1193–1200.

Peresson, H. and Decker, K., 1997a. Far-field effects of Late Miocene subduction in the Eastern Carpathians: E–W compression and inversion of structures in the Alpine–Carpathian–Pannonian region. Tectonics, 16, 38–56.

Peresson, H. and Decker, K., 1997b. The Tertiary dynamics of the northern Eastern Alps (Austria): changing paleostress in a collisional plate boundary. Tectonophysics, 272, 125–157.

Petit, J.P., 1987. Criteria for the sense of movement on fault surfaces in brittle rocks. Journal of Structural Geology, 9, 597– 608.

Pichler, H., 1963. Geologische Untersuchungen im Gebiet zwischen Rossfeld und Markt Schellenberg im Berchtesgadener Land. Beihefte zum Geologischen Jahrbuch, 48, 29–204.

Plöchinger, B., 1984. Zum Nachweis jurassischer-kretazischer Eingleitungen von Hallstätter Gesteinsmassen beiderseits des Salzach-Quertales (Salzburg). Geologische Rundschau, 73/1, 293–306.

Plöchinger, B., 1987. Geologische Karte der Republik Österreich 1:50.000, Blatt 94 Hallein. Geologische Bundesanstalt, Wien.

Plöchinger, B. (with contributions by H. Brandecker, H.P. Leditzky, V. Maurin, G. Tichy, D. van Husen) 1990. Erläuterungen zu Blatt 94 Hallein. Geologische Bundesanstalt, Vienna, pp. 76.

Pueyo, E.L., Mauritsch, H.J., Gawlick, H.-J., Scholger, R. and Frisch, W., 2007. New evidence for block and thrust sheet rotations in the central northern Calcareous Alps deduced from two pervasive remagnetization events. Tectonics, 26, doi: 10.1029/2006TC001965.

Ratschbacher, L., 1986. Kinematics of Austro-Alpine cover nappes: changing translation path due to transpression. Tectonophysics, 125, 335–356.

Ratschbacher, L., Frisch, W., Linzer, G. and Merle, O. 1991. Lateral extrusion in the Eastern Alps, part 2: Structural analysis. Tectonics, 10, 257–271.

Ratschbacher, L., Frisch, W., Neubauer, F., Schmid, S.M. and Neugebauer, J., 1989. Extension in compressional orogenic belts: The eastern Alps. Geology, 17, 404–407.

Ratschbacher, L. and Neubauer, F., 1989. West-directed decollement of Austro-Alpine cover nappes in the eastern Alps: geometrical and rheological considerations. Geological Society, London, Special Publication, 243–262.

Rouby, D., Raillard, S., Guillocheau, F., Bouroullec, R. and Nalpas, T., 2002. Kinematics of a growth/raft system on the West African margin using 3-D restoration. Journal of Structural Geology, 24, 783–796.

Sachsenhofer, R.F., Lankreijer, A., Cloetingh, S. and Ebner, F., 1997. Subsidence analysis and quantitative basin modelling in the Styrian Basin (Pannonian Basin System, Austria). Tectonophysics, 272, 175–196.

Schauberger, O., 1986. Bau und Bildung der Salzlagerstätten des ostalpinen Salinars. Archiv für Lagerstättenforschung der Geologischen Bundesanstalt, 7, 217–254.

Schorn, A., Neubauer, F., Genser, J. and Bernroider, M. (submitted). The Haselgebirge evaporitic mélange in central Northern Calcareous Alps (Austria): part of the Permian rift of the Meliata ocean? Tectonophysics.

Schorn, A., 2010. The sulphatic Haselgebirge evaporite mélange revisited: evidence from the Moosegg quarry within central Northern Calcareous Alps. Unpub. MSc thesis, faculty of Sciences, University of Salzburg, pp. 139.

Schweigl, J. and Neubauer, F., 1997. Structural development of the central Northern Calcareous Alps: Significance for the Jurassic to Tertiary geodynamics in the Alps. Eclogae Geologia Helvetica, 60, 303–323.

Spang, J. H., 1972. Numerical Method for Dynamic Analysis of Calcite Twin Lamellae. Geological Society of America Bulletin, 83, 467–472.

Spötl, C., Kralik, M., Kunk, M.J., 1996. Authigenic Feldspar as an Indicator of Paleo-Rock/Water Intercalations in Permian Carbonates of the Northern Calcareous Alps, Austria. Journal of Sedimentary Research, 66, 139–146.

Spötl, C., Kunk, M.J., Ramseyer, K. and Longstaffe, F.J., 1998a. Authigenic potassium feldspar: a tracer for the timing of palaeofluid flow in carbonate rocks, Northern Calcareous Alps, Austria. In: Parnell, J. (ed.) Dating and Duration of Fluid Flow and Fluid-Rock Interaction. Geological Society [London] Special Publication, 144, pp. 107–128.

Spötl, C., Longstaffe, F.J., Ramseyer, K., Kunk, M.J., Wiesheu, R., 1998b. Fluid-rock reactions in an evaporitic mélange, Permian Haselgebirge, Austrian Alps. Sedimentology, 45, 1019– 1044.

Tollmann, A, 1985. Geologie von Österreich. Außerzentralalpiner Anteil Deuticke, Wien, pp. XV+710.

Tollmann, A., 1987. Late Jurassic/Neocomian Gravitational Tectonics in the Northern Calcareous Alps in Austria. In: Flügel, H.W. and Faupl, P. (eds.) Geodynamics of the Eastern Alps. Deuticke, Wien, pp. 112–125.

Twiss, R.J. and Unruh, J.R., 1998. Analysis of fault slip inversions: Do they constrain stress or strain rate? Journal of Geophysical Research, 103, 12,205–12,222.

Wagreich, M. and Decker, K., 2001. Sedimentary tectonics and subsidence modelling of the type Upper Cretaceous Gosau basin (Northern Calcareous Alps, Austria), International Journal of Earth Sciences (Geologische Rundschau), 90, 714–726.

Wang, X. and Neubauer, F. 1998. Orogen-parallel strike-slip faults bordering metamorphic core complexes: the Salzach-Enns fault zone in the Eastern Alps, Austria. Journal of Structural Geology, 20, 799–818.

Wiesheu, R., 1997. Geologisch-geochemische Untersuchungen zur Rekonstruktion der thermischen Geschichte des Haselgebirges. 95 p., Dissertation, University TU München, Hieronymus, München.

Received: 13 August 2011
Accepted: 31 October 2011

Anja SCHORN*) & Franz NEUBAUER

Dept. Geography and Geology, University of Salzburg, Hellbrunnerstr. 34, A-5020 Salzburg, Austria;

*) Corresponding author, anja.schorn2@stud.sbg.ac.at

Appendix

Palaeostress techniques

A list of stations is given in Tables 1 (surroundings of the Moosegg quarry) and 2 (Moosegg quarry). In many outcrops, superimposed sets of slickensides and striations indicate a polyphase reactivation of these faults. However, some uncertainties of relative chronology remain. The determination of the succession of faulting and of displacement followed criteria proposed by, e.g. Petit (1987) and Gamond (1983, 1987). Paleostress orientation patterns were evaluated from this fault and slickenside data using numerical and graphical inversion methods proposed by Angelier and Méchler (1977), Angelier (1979, 1989), Armijo et al. (1982) and Marret and Almendinger (1990). These inversion methods indicate strain rather than paleostress patterns with relative magnitudes of principal stress axes (Twiss and Unruh 1998). Although the rocks are generally anisotropic, we report the R-value of the paleostress tensor because present versions of paleostress inversion techniques calculate the appropriate R-value only for isotropic material. Two numerical methods for calculating paleostress tensors were used in this study: NDA (Numerical Dynamic Analysis; Spang, 1972) and direct inversion (Angelier, 1979). The NDA method calculates the orientation of the principal axes of the paleostress tensor from summation of individual tensors for every plane. The direct inversion method minimizes the angles between the calculated directions of maximum shear stress acting along the fault plane and the measured striation, which leads to the determination of the reduced stress tensor defined by the orientation of the principal stress axes and the stress ratio (Ortner et al., 2002). In both cases, the orientation and relative values of the principal stresses are derived from the eigen values and eigen vectors of the bulk stress tensor. The quality of the calculation is checked in the normalized Mohr circle plot for three-dimensional stresses. At least four independent fault planes are required for the calculation of the NDA and inversion method. In cases where less than four independent fault planes were available, we used the dihedra method of Angelier and Mechler (1977). Although it is known that from a purely statistical point of view, a tensor solution based on less than four independent, differently oriented, fault planes is meaningless because the solution space is not completely determined, we used the solutions in these cases as a reference in some areas. The age of each measured rock together with the principal orientation for each phase of deformation is given in Tables 1 and 2.